



1 Measurement of ambient NO₃ reactivity: Design, characterization 2 and first deployment of a new instrument

3 Jonathan M. Liebmann¹, Gerhard Schuster¹, Jan B. Schuladen¹, Nicolas Sobanski¹, Jos Lelieveld¹ and
4 John N. Crowley¹

5 ¹Atmospheric Chemistry Department, Max-Planck-Institut für Chemie, 55128 Mainz, Germany.

6 *Correspondence to:* John N. Crowley (john.crowley@mpic.de)

7 **Abstract.** We describe the first instrument for measurement of the rate constant (s^{-1}) for reactive loss (i.e. the total reactivity)
8 of NO₃ in ambient air. Cavity-ring-down spectroscopy is used to monitor the mixing ratio of synthetically generated NO₃ (\approx
9 30-50 pptv) after passing through a flow-tube reactor with variable residence time (generally 10.5 s). The change in
10 concentration of NO₃ upon modulation of the bath gas between zero-air and ambient air is used to derive its loss rate
11 constant, which is then corrected for formation and decomposition of N₂O₅ via numerical simulation. The instrument is
12 calibrated and characterized using known amounts of NO and NO₂ and tested in the laboratory with an isoprene standard.
13 The lowest reactivity that can be detected (defined by the stability of the NO₃ source, instrumental parameters and NO₂
14 mixing ratios) is 0.005 s⁻¹. An automated dilution procedure enables measurement of NO₃ reactivities up to 45 s⁻¹, this upper
15 limit being defined mainly by the dilution accuracy. The typical total uncertainty associated with the reactivity measurement
16 at the centre of its dynamic range is 16 %, though this is dependent on ambient NO₂ levels. Results from the first successful
17 deployment of the instrument at a forested mountain site with urban influence are shown and future developments outlined.

18



19 1 Introduction

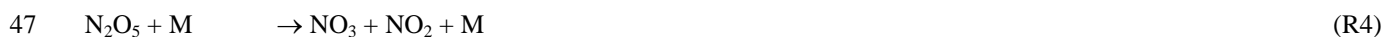
20 Large amounts of biogenic and anthropogenic trace gases are emitted annually into the atmosphere. Recent estimates
 21 (Guenther et al., 2012) suggest that about 1000 Tg of biogenic volatile organic compounds (bVOC), especially isoprene
 22 (contributing 50 %) and monoterpenes (15 %) are emitted annually by vegetation. The global burden of anthropogenic
 23 emission is dominated by CO₂, CO, N₂O, CH₄, SO₂, NO₂ and organic carbon, the latter contributing about 11 Tg (Huang et
 24 al., 2015). In particular, nitrogen oxides from combustion and microbial activity in soils have a major impact on the
 25 chemistry of the natural atmosphere (Crutzen, 1973). Most VOCs are oxidized efficiently in the Earth's boundary layer, the
 26 oxidizing capacity of which represents 15% of that of the entire atmosphere (Lelieveld et al., 2016). Biogenic and
 27 anthropogenic VOCs have a significant impact on air quality and human health and knowing and understanding their
 28 lifetimes, which are determined by the oxidizing capacity of the atmosphere, is prerequisite to predicting future atmospheric
 29 composition and related climate phenomena (Lelieveld et al., 2008).

30 During day-time, photo-chemically formed OH radicals represent the dominant contribution to the oxidative capacity of the
 31 atmosphere. As OH levels are vastly reduced in the absence of sunlight, the NO₃ radical (formed by reaction of NO₂ with O₃,
 32 R1) is the major oxidizing agent for many biogenic terpenoids and other unsaturated compounds at night-time (Brown and
 33 Stutz, 2012; Ng et al., 2016; Wayne et al., 1991; Atkinson, 2000; Atkinson and Arey, 2003a, b).



35 NO₃ reacts rapidly with NO (R2, rate constant 2.6 × 10⁻¹¹ cm³ molecule⁻¹ s⁻² at 298 K (Atkinson et al., 2004)) and undergoes
 36 rapid photolysis (R5, R6) so that its lifetime is usually of the order of seconds during the day and its concentration too low
 37 for it to be considered an important day-time oxidant.

38 At night, NO₃ can react with NO₂ forming N₂O₅, which thermally decomposes to set up a thermal equilibrium between NO₂,
 39 NO₃ and N₂O₅ (R3, R4) with N₂O₅ formation favoured by lower temperatures. As both NO₃ and N₂O₅ are formed from NO_x
 40 (NO_x = NO + NO₂) the loss of either NO₃ via gas-phase losses or N₂O₅ via heterogeneous uptake to particles or deposition
 41 implies a reduction in NO_x, and thus a reduction in the rate of photochemical O₃ formation (Dentener and Crutzen, 1993). In
 42 addition, heterogeneous loss of N₂O₅ can also result in release of ClNO₂ from chloride containing particles (R7) (Phillips et
 43 al., 2012; Mielke et al., 2011; Osthoff et al., 2008; Riedel et al., 2012; Thornton et al., 2010). The main loss processes of
 44 NO₃ are summarised in Fig. 1.





51 In rural and forested areas reaction with biogenic VOCs can dominate the loss of NO_3 (Mogensen et al., 2015). Especially
52 terpenoids like limonene ($k = 1.2 \times 10^{-11} \text{ cm}^3 \text{ molecule}^{-1} \text{ s}^{-1}$), α -pinene ($k = 6.2 \times 10^{-12} \text{ cm}^3 \text{ molecule}^{-1} \text{ s}^{-1}$) and isoprene ($k =$
53 $6.5 \times 10^{-13} \text{ cm}^3 \text{ molecule}^{-1} \text{ s}^{-1}$) have high rate constants for reaction with NO_3 (IUPAC, 2016; Ng et al., 2016). Under such
54 conditions, when NO_x levels are low, NO_3 mixing ratios may be sub-pptv and below the detection limit for most instruments
55 (Rinne et al., 2012).

56 The reaction of NO_3 with traces gases containing unsaturated C=C bonds proceeds via addition to form nitroxy-alkyl radicals
57 that undergo rapid reaction with O_2 to form nitroxy-alkyl peroxy radicals. The peroxy radicals react further (with HO_2 , NO ,
58 NO_2 or NO_3), to form multi-functional organic nitrates, which can contribute to generation and growth of secondary organic
59 aerosols (Fry et al., 2014; Ng et al., 2016) or be lost by deposition.

60 The role of NO_3 as an oxidizing agent may be assessed via its total reactivity (or inverse lifetime). Whereas for OH,
61 experimental methods for measuring total reactivity in ambient air exist (Kovacs and Brune, 2001; Sinha et al., 2008), NO_3
62 reactivity has not yet been directly measured. Stationary-state approximations have often been used to calculate NO_3
63 lifetimes from its mixing ratio and production rate, the latter being given by: $k_1[\text{NO}_2][\text{O}_3]$ (Sobanski et al., 2016b; Brown et
64 al., 2009; Brown et al., 2007a; Brown et al., 2007b; Geyer and Platt, 2002; Heintz et al., 1996). Thus the stationary-state
65 turnover lifetime, τ_{ss} , can be calculated according to expression 1.

$$66 \quad k_{ss} = \frac{1}{\tau_{ss}} = \frac{[\text{NO}_3]}{k_1[\text{O}_3][\text{NO}_2]} \quad (1)$$

67 This method is applicable when the chemical lifetime of NO_3 is sufficiently short so that stationary-state can be achieved
68 within transport time from emission to measurement location (Brown et al., 2003). Formally it is achieved when the
69 production and loss of NO_3 and N_2O_5 are balanced (Brown et al., 2003; Crowley et al., 2011). The time to acquire stationary-
70 state depends on production and loss rates for NO_3 and N_2O_5 and can take several hours. This approach can break down
71 under conditions of moderate to high NO_2 levels, strong sinks, low temperatures, or very clean air masses in which the sinks
72 for NO_3 and N_2O_5 become small (Brown et al., 2003). Indeed, Sobanski et al. (2016b) observed much lower stationary-state
73 loss rates compared to those calculated from measured VOC mixing ratios during the PARADE 2011 campaign and
74 concluded that this was mainly the result of sampling from a low lying residual layer with VOC emissions that were too
75 close for NO_3 concentrations to achieve stationary-state. They also considered the possibility that NO_3 may be formed by the
76 oxidation of NO_2 by Criegee Intermediates, which would bias calculations of its reactivity.

77 Summarizing, NO_3 reactivity with respect to gas-phase losses is a direct indication of night-time oxidation rates of VOCs,
78 with direct impacts on NO_x levels by forming long-lived reservoir species (alkyl nitrates) some of which will partition to the
79 particle phase. Via modification of N_2O_5 concentrations, the NO_3 reactivity indirectly controls heterogeneous NO_x losses and
80 ClNO_2 formation rates.

81 In this paper we describe a newly developed instrument that enables point measurements of NO_3 reactivity in ambient air.
82 After introducing the methodology in section 2, we show the results of extensive laboratory characterization of the



83 instrument along with discussion of the uncertainties associated with those measurements in section 3 to 5. In section 6 we
84 present a dataset of ambient NO_3 reactivity obtained at a forested / urban location in south-western Germany.

85 **2 Methodology**

86 Our experiments to measure NO_3 reactivity involve comparison of loss rates of synthetically generated NO_3 in zero-air and
87 in ambient air introduced into a flow-tube reactor. In zero-air, the loss of NO_3 is due to its reaction with NO_2 (present as a
88 necessary component in the generation of NO_3 , see below) and losses on surfaces of the flow-tube. When zero-air is replaced
89 by ambient air, NO_3 is additionally removed by reaction with reactive gases present and its mixing ratio reduced accordingly.
90 An analysis of the change in signal for a fixed reaction time enables the NO_3 reactivity to be derived once certain corrections
91 have been applied (see below).

92 Figure 2 displays a schematic diagram of the experimental set-up. The three central components are a dark reactor for
93 generation of NO_3 , the flow-tube in which NO_3 reacts with trace gases in ambient air samples and the detection system for
94 NO_3 .

95 **2.1 Generation of NO_3**

96 Many laboratory studies of NO_3 kinetics have used the thermal decomposition of N_2O_5 as NO_3 source (R4) (Wayne et al.,
97 1991). The generation of NO_3 from gas-phase N_2O_5 eluted from samples of crystalline N_2O_5 (at $-80\text{ }^\circ\text{C}$) was found to be
98 insufficiently stable for the present application and is also difficult to use during field campaigns where adequate laboratory
99 facilities for the safe generation and purification of N_2O_5 are frequently not available. In addition, this method of NO_3
100 generation was also accompanied by an NO_2 impurity of several parts per billion (ppbv).

101 We therefore generate NO_3 and N_2O_5 in situ, via the oxidation of NO_2 by O_3 (R1, R3). For this purpose, 400 standard cm^3
102 min^{-1} (sccm) of synthetic air from a zero-air generator (Fuhr Cap 180) are passed over a Hg lamp (low-pressure, Penray type)
103 at a pressure of 1200 Torr. The photo-dissociation of O_2 at 184.95 nm results in formation of oxygen atoms that recombine
104 with O_2 to form ≈ 400 ppbv O_3 . The O_3 / air flow is then mixed with NO_2 in synthetic air (0.93 ppbv, 1-10 sccm) and
105 directed into a temperature stabilized ($30\text{ }^\circ\text{C}$), darkened, FEP coated reactor (length 70 cm, diameter 6 cm) also at a pressure
106 of 1200 Torr. The reactor is darkened to prevent the photolysis of NO_3 by room lights. Operation at above-ambient pressure
107 extends the reaction time for a given flow rate, thus optimising the conversion of NO_2 to NO_3 via the reaction between NO_2
108 and O_3 , which has a low rate constant of $4.05 \times 10^{-17}\text{ cm}^3\text{ molecule}^{-1}\text{ s}^{-1}$ at $30\text{ }^\circ\text{C}$. The use of high pressures also optimises the
109 formation of N_2O_5 in the termolecular reaction R3, and reduces the rate of diffusion and loss of NO_3 to the walls of the
110 reactor. A high pressure in the darkened reactor also has the advantage of decoupling it from fluctuations in ambient
111 pressure, which influence the formation of N_2O_5 . Heating the reactor to above room-temperature is carried out to stabilise the
112 formation of N_2O_5 , which otherwise shows strong fluctuations owing to variations in laboratory temperature, typically about



113 3-5 degrees within the course of a day or night. The approximate reaction time for the stepwise conversion of NO_2 to N_2O_5 in
114 the darkened reactor is ≈ 5 min.

115 The gas exiting the darkened reactor passes through a pin-hole ($\varnothing \approx 250 \mu\text{m}$) to reduce the pressure to roughly ambient level
116 and then enters a ≈ 30 cm long piece of $\frac{1}{4}$ inch (≈ 6.4 mm) PFA tubing (residence time ≈ 0.5 s) which is heated to 140°C in
117 order to thermally decompose N_2O_5 to NO_3 . Calculations using the thermal decomposition rate constant for N_2O_5 (lifetime =
118 0.001 s at 140°C) indicate that after ≈ 0.1 s the N_2O_5 is stoichiometrically converted to NO_3 . The temperature is measured on
119 the outside of the PFA tubing and does not necessarily reflect the temperature of the gas flowing through it. The value of
120 140°C is chosen based on a series of experiments in which the tubing temperature was varied and the yield of NO_3
121 monitored. A PFA T-piece located immediately behind the heated tubing is used to add a 2900 sccm flow of either zero- or
122 ambient-air to the synthetic NO_3 sample. After this dilution step the air contains ≈ 50 pptv NO_3 , ≈ 1 ppbv NO_2 and ≈ 50 ppbv
123 O_3 . As described later, keeping NO_2 and O_3 levels as low as possible has important consequences for the data analysis. Low
124 levels of NO_3 also help to ensure that the addition of NO_3 does not significantly change the reactivity of the air, i.e. by
125 removing a large fraction of the reactive trace gases.

126 As described below, the present instrument is a modification of one designed to measure ambient mixing ratios of NO_3 and
127 N_2O_5 and is equipped with a second cavity connected to a heated inlet that measures the sum of NO_3 and N_2O_5 . Experiments
128 in which both cavities were used to analyze the flow out of the heated piping indicated that there was no residual N_2O_5 .

129 **2.2 Detection of NO_3 using cavity-ring-down spectroscopy**

130 For detection of the NO_3 radical we used Cavity Ring-Down Spectroscopy (CRDS), a sensitive technique for measurements
131 of atmospheric trace gases and often used for measurement of ambient NO_3 (Brown et al., 2002). In essence, CRDS is an
132 extinction measurement in a closed optical resonator (cavity) where light is trapped between mirrors with high reflectivity to
133 generate a very long absorption path. Ring-down refers to the decay of light intensity (monitored behind the cavity exit
134 mirror) and the general expression to derive the concentration of an absorbing or scattering gas is given by (Berden et al.,
135 2000):

$$136 \quad [\text{X}] = \frac{1}{c\sigma_{(X,\lambda)}} \left(\frac{1}{\tau_X} - \frac{1}{\tau_0} \right) \quad (2)$$

137 Where τ_0 and τ_X correspond to decay constants in the absence and presence of an absorbing or scattering trace gas X,
138 respectively and $\sigma_{(X,\lambda)}$ is the absorption cross-section / scattering coefficient of X at wavelength λ .

139 The instrument used is a two-channel CRDS that was previously used to measure ambient levels of N_2O_5 and NO_3 (Crowley
140 et al., 2010; Schuster et al., 2009). Important modifications to the previous set-up include use of FEP coated glass cavities of
141 equivalent size and fibre-optics for the coupling of the laser to the cavity. The thermal dissociation cavity previously used for
142 detection of atmospheric N_2O_5 is not necessary for the measurement of NO_3 lifetimes but was used for calibration and
143 characterization experiments. Only the central features and important modifications compared to the prototype described in
144 Schuster et al., (2009) are described in detail here.



145 The light source is a 625 Hz, square-wave modulated, 100 mW laser-diode located in a Thor Labs TCLDM9 housing and
146 thermally stabilized at 36°C using a Thor Labs ITC 502 Laser-Diode Combi Controller to produce light at 661.95 nm (0.5
147 nm full width at half maximum) and therefore close to the NO₃ absorption maximum. The effective cross section of NO₃ was
148 calculated as $2.09 \times 10^{-17} \text{ cm}^2 \text{ molecule}^{-1}$ by convoluting the temperature dependent NO₃ absorption spectrum (Orphal et al.,
149 2003; Osthoff et al., 2007) with the laser-diode emission spectrum. Coupling between the laser-diode and the cavities is
150 achieved by using either optical fibres (0.22 NA, 50 µm core, 400-2400 nm) for measuring NO₃ reactivity or using fibre-
151 optics with a beam splitter (Thor Labs FCMM50-50A-FC, 50:50 ratio) in order to operate both cavities. The beam was
152 collimated (Thor Labs FiberPort Collimator PAF-X-18-PC-A) and directed through an optical isolator (Thorlabs IO-3D-660-
153 VLP), focused by a lens (Thorlabs A230TM-A) into the optical-fibre and then collimated again to a beam diameter of about
154 6 mm before entering the cavity.

155 The NO₃ cavity (Teflon-coated glass (DuPont, FEP, TE 9568), length 70 cm, volume 79cm³) was operated at room
156 temperature, while the N₂O₅ cavity was operated at 80°C with a pre-cavity section heated to 85°C in order to convert N₂O₅ to
157 NO₃. The NO₃-cavity was connected to the flow-tube using 1/8" (≈ 3.2 mm) PFA tubing that lined the 1/4" (≈ 6.4 mm)
158 injector. The use of small diameter tubing results in short transport times between the flow-tube and CRDS and also induces
159 a pressure drop of 133 mbar, so that the pressure in the cavity was 880 mbar. Gases entered the middle of the cavity via a T-
160 piece and were pumped from the ends via a flow controller into the exhaust. The flow rates in both cavities were 3000 cm³
161 (STP) min⁻¹ (sccm) resulting in a residence time of approximately 1.6 s as calculated from the volume flow. Gas entering the
162 CRDS detector was always passed through a 2 µm membrane filter (Pall Teflo) to remove particles. Light exiting the cavities
163 through the rear mirror was detected by a photomultiplier (Hamamatsu E717-500) which was screened by a 662 nm
164 interference filter. The pre-amplified PMT signal was digitized and averaged with a 10 MHz, 12 bit USB scope (Picoscope
165 3424) which was triggered at the laser modulation frequency of 625 Hz.

166 The ring-down constant in the absence of NO₃ was obtained by adding NO (1-3 sccm of a 100 ppmv mixture NO in N₂)
167 every 40 points of measurement for approximately 15 s. Titration with NO took place at the inlet of the T-shaped glass
168 cavity giving the gas mixture sufficient time to react with NO₃. The L/d ratio (the ratio of the distance between the cavity
169 mirrors (L) and the length of the cavity that is filled by absorber (d)) was determined as described previously (Schuster et al.,
170 2009; Crowley et al., 2010) and was 1.01 ± 0.03 . Values of τ_0 in dry zero-air at 760 Torr were usually between 140 and
171 160 µs indicating optical path lengths of ≈ 42-48 km. When operated at a flow of 3000 sccm, the noise levels on the NO₃
172 signal are such that the precision (3s integration interval) is better than 1 pptv. As we describe later, the NO₃ reactivity is
173 derived from measurements of the relative change in the NO₃ mixing ratio, so that the precision rather than total uncertainty
174 in the NO₃ mixing ratio defines the accuracy of the reactivity measurement.

175



176 2.3 Flow-tube for NO₃ reactivity measurement

177 The flow-tube, thermostatted to 20 °C by flowing water through an outer jacket, is an FEP-coated glass tube of length 50 cm
178 and internal diameter 4 cm. Gas enters the flow-tube at one end via a conical section with a 3/8 inch (≈ 9.5 mm) glass fitting
179 through which ¼ inch (≈ 6.4 mm) PFA tubing could be inserted. The total flow through the flow-tube was 3300 sccm,
180 consisting of 400 sccm from the darkened reactor and 2900 sccm zero-air / ambient air. The flow and pressures indicated
181 above, result in a Reynolds number of ≈ 123 (i.e. laminar flow) in the cylindrical part of the flow-tube, but with an entrance
182 length (Le) to acquire laminar flow of 27 cm indicating that the flow-tube operates in a mixed turbulent / laminar flow
183 regime.

$$184 \quad Le = 0.112 r Re \quad (3)$$

185 Gases exit the flow-tube via a length of 1/8 inch PFA tubing supported in an axially centred stainless-steel tube (length 50
186 cm, diameter ¼ inch) which could be translated along the major flow-tube axis thus changing the contact (reaction) time
187 between NO₃ and any reactive species or the flow-tube wall. In principal, this enables the dynamic range of the measurement
188 to be adjusted (i.e. long contact times for low reactivity, short contact times for high reactivity) though we found that
189 reactivity-dependent dilution of the ambient air was a better method to extend the dynamic range to high reactivities as very
190 short reaction times were not possible due to a finite residence time in the CRDS detection system and also due to mixing
191 effects in the flow-tube. In order to prevent formation of a “dead volume” at the back of the flow-tube beyond the tip of the
192 outlet, 400 sccm were removed via a critical orifice to the exhaust pump. During measurement of NO₃ reactivity the
193 extraction point was usually set for a reaction time of about 10.5 s, which was determined as described below.

194 As described later, to derive the NO₃ reactivity we compare its concentration in zero-air to that in ambient air samples. We
195 found that when switching between sampling ambient air and dry, zero-air, the resulting change in relative humidity caused
196 an abrupt change in NO₃ which then slowly recovered towards its original value. Measurement of the wall loss rate of NO₃
197 in dry and humidified zero-air by moving the injector (see below) revealed no substantial difference and we conclude that
198 the change in NO₃ is due to wall loss at the point of mixing of NO₃ flows and the zero-air flow, which is very turbulent. In
199 order to eliminate data loss while waiting for signals to stabilise following zeroing, we humidify the zero-air to the same
200 absolute humidity (±2 %) as ambient. To do this, the ambient relative humidity was monitored by passing 100 sccm air over
201 a sensor that recorded both temperature and relative humidity. The zero-air was humidified by directing a variable fraction of
202 the (constant) total flow through a 2 l gas wash-bottle filled with HPLC grade water. The relative humidity of the resulting
203 mixture was matched to ambient levels by dynamic adjustment of the fractional flow passing through the wash-bottle. The
204 zero-air used for purging the mirrors as well that used for NO₃ generation was not humidified.

205 In order to ensure that air from the zero-air generator was free of reactive gases that survived the catalytic purification
206 process, we compared it to hydrocarbon-free, bottled synthetic air (Westfalen). No change in the concentration of [NO₃]
207 could be observed when switching between zero-air and bottled air, indicating that the zero-air generator was suitable.



208 However, poisoning of the catalyst of the zero-air generator by amines, sulphides or thiols or contamination of the filters
209 could potentially become problematic when using compressed, highly polluted ambient air.

210 **2.3.1 Derivation of the effective reaction time and wall loss rate constant for NO₃**

211 In flow-tubes where radial, diffusive mixing of gases is rapid (i.e. at low pressures of He and “plug-flow” conditions), the
212 effective reaction time can be close to that calculated from the volumetric flow rate once axial diffusion is accounted for
213 (Howard, 1979). At higher pressures and laminar flow, reactions times are defined by the parabolic velocity distribution and
214 extent of radial mixing whereas high pressure flow-tubes operated under turbulent conditions (Reynold numbers > 3000)
215 plug-flow can be achieved (Donahue et al., 1996; Seeley et al., 1993). According to the calculations of Reynolds numbers
216 outlined above, our flow-tube is not operated in either a pure laminar or turbulent regime, which can make accurate
217 calculation of the reaction time difficult. Using the volumetric flow rate and flow-tube diameter, we calculate an average,
218 linear velocity of the gas of 4.78 cm s⁻¹ at 760 Torr and 298 K in the cylindrical section of the flow-tube. This enables us to
219 calculate the injector position dependent reaction time in the flow-tube, which for 45 cm is 9.5 s. This should be regarded as
220 an initial estimate of the true reaction time as it does not consider the non cylindrical section of the flow-tube (2.5 % of total
221 volume), the radial distribution of velocities in the flow-tube or mixing effects. A further additional 1.6 s must be added to
222 this to take the average reaction time in the cavity into account (calculated from the cavity volume and the flowrate) resulting
223 in an approximate, total reaction time of 11.1 s.

224 A further method to derive an “effective” or averaged reaction time is to add a short pulse of gas to the flow-tube and
225 monitor its arrival time at the detector. However, as NO₃ cannot be easily stored, we instead add a pulse of a reactant that
226 removes NO₃. A syringe was therefore used to add a short pulse (0.1 cm³ in < 0.5 s) of NO diluted in N₂ (0.22 ppbv) to the
227 flow-tube at the T-piece where the NO₃ source and zero-air are mixed.

228 The resultant depletion in the NO₃ signal (measured at a time resolution of 0.35 s) displayed an inverted Gaussian form with
229 an elongated flank after the minimum (Fig. 3) which can be attributed to non-isothermal effects, secondary flows and
230 recirculation processes in the flow-tube (Huang et al., 2016) which require fluid dynamics simulations to be fully
231 characterised. The average reaction time, t , can however be derived from:

$$232 \quad t = \frac{\sum I_j t_j}{\sum I_j} \quad (4)$$

233 where I_j is the signal recorded at each time step t_j

234 In total, 25 experiments were conducted, resulting in an effective reaction time of 11.4 ± 0.5 s determined via expression (4).
235 The two methods outlined above thus provide approximate values for the reaction time which are in good agreement (< 3 %
236 deviation).

237 As the reaction time is a central parameter for calculating the NO₃ reactivity, a third method was employed, in which a
238 known amount of NO was added at the usual mixing point and the depletion in NO₃ observed. As the rate constant for
239 reaction of NO with NO₃ is known with an uncertainty (at room temperature) of 13 %, this should enable derivation of an



240 effective reaction time that also takes all mixing effects (both in the flow-tube and cavity) into account. In a series of
 241 experiments, known amounts NO were added to the 2900 sccm flow of zero-air (via a calibrated mass flow controller) at the
 242 usual mixing point. In the absence of other processes which remove or form NO₃, its change in concentration upon adding
 243 NO is described by:

$$244 \quad [\text{NO}_3]_t = [\text{NO}_3]_0 \exp^{-(k_2[\text{NO}] + k_w + k_3[\text{NO}_2])t} \quad (5)$$

245 Where [NO₃]₀ and [NO₃]_t are the concentrations of NO₃ before and after addition of NO, respectively. *k*₂ and *k*₃ are the rate
 246 constants for reaction of NO₃ with NO and NO₂, respectively at the flow-tube / cavity temperature, *k*_w is the rate constant (s⁻¹)
 247 for loss of NO₃ at the flow-tube walls and *t* is the desired parameter. Rearranging, we get a simple expression (6), which
 248 shows that a plot of ln([NO₃]_t) versus [NO] should yield a slope of *k*₂*t*, from which *t* can be derived using an evaluated and
 249 recommended value of *k*₂ (Atkinson et al., 2004). Once corrected for the contribution from *k*₃[NO₂], the intercept should, in
 250 principal, give a value of *k*_w.

$$251 \quad \ln \frac{[\text{NO}_3]_0}{[\text{NO}_3]_t} = k_2[\text{NO}]t + k_w + k_3[\text{NO}_2] \quad (6)$$

252 A plot of [NO₃]_t versus [NO] is displayed in Fig. 4a for three different amounts of added NO₂. Although the curve follows
 253 roughly exponential behaviour as expected, the slopes and thus the value of *t* obtained was found to depend on the initial
 254 NO₂ concentration, with values of 5.7, 5.1 and 4.5 s obtained for NO₂ mixing ratios of 2.94, 5.88 and 8.82 ppbv,
 255 respectively. This indicates that the kinetics of NO₃ formation and loss are more complex than defined by expression (6) and
 256 the relative rates of reaction of NO₃ with NO (R2) and NO₂ (R3) and its formation via N₂O₅ decomposition (R4) and reaction
 257 of O₃ with NO₂ (R1) in the flow-tube all impact on the NO₃ mixing ratio. In Fig. 4b we display the results of a similar
 258 experiment in which NO₂ as added. In this case, there is obvious curvature in the plot of [NO₃]_t versus [NO₂], which is not
 259 predicted by expression (5). The decomposition of N₂O₅ formed by reaction R3 as well as oxidation of NO₂ by O₃ (R1, see
 260 section 3.1) both lead to the formation of NO₃ and are the causes of this behaviour, especially at high [NO₂] and low [NO].
 261 At the flow-tube and cavity temperature (circa 298 K), the rate constant for decomposition of N₂O₅ (*k*₄) is 4.4x10⁻² s⁻¹
 262 (Atkinson et al., 2004).

263 Extraction of the reaction time thus required numerical simulation of the data obtained by adding various amounts of NO, to
 264 the flow-tube in the presence of different NO₃ and NO₂ concentrations. The impact of reactions R2, R3 and R4 was assessed
 265 by numerical simulations using FACSIMILE (Curtis and Sweetenham, 1987) and considering the reactions listed in Table 1.
 266 The input parameters for the simulations were the concentrations of NO, NO₂ and O₃ and the rate constants, which were
 267 taken from IUPAC recommendations (Atkinson et al., 2004). The total reaction time (*t*) and the wall-loss rate constant for
 268 NO₃ (*k*_w) were adjusted until each of the six datasets could be reproduced with a single value for each parameter. The initial
 269 concentration of [NO₃]₀, was allowed to float until best agreement was achieved. This way, the reaction time was determined
 270 to be 10.5 s, which is in good agreement with that derived by pulsed addition of NO. As our reactivity derivation relies on
 271 the change in NO₃ signal upon adding a reactant to the flow-tube, we consider the value of 10.5 s, which takes mixing,



272 diffusion etc. into account to be the most appropriate value but assign an uncertainty (± 1 s) that overlaps with the other
 273 methods. The wall loss rate of NO_3 (which is independent of the NO and NO_2 concentrations) was found to be $4 \times 10^{-3} \text{ s}^{-1}$.
 274 For analysis of ambient reactivity we use a reaction time of 10.5 s as derived from the addition of NO . This means that our
 275 ambient reactivities are directly tied to the rate constant for reaction between NO_3 and NO . As described later, during
 276 ambient measurements we periodically add a known amount of NO to the zero-air to monitor a known reactivity under real
 277 operating conditions.

278 Figures 5a and 5b show the correlation between simulated and measured NO_3 concentrations in these experiments. In both
 279 cases the slope is close to unity (0.97-1.02) with an intercept close to zero. A set of similar experiments performed at 30 %
 280 and 80 % humidity also showed excellent agreement using the same values of t and k_w . We conclude that the behaviour of
 281 NO_3 in this system can be very accurately predicted by numerical simulations using a simple reaction scheme under a variety
 282 of conditions (initial NO_3 , NO and NO_2 varied), giving us confidence in our ability to extract loss rates for NO_3 in ambient
 283 air.

284 When gas-phase reactivity is low, a substantial fraction of NO_3 may be lost via collisions with the walls rather than due to
 285 reactive gases. For this reason, we re-measured the value of k_w obtained above in a further set of experiments in which the
 286 NO_3 concentration was measured as a function of injector position (contact time in the flow-tube) at a constant initial mixing
 287 ratio of NO_3 and NO_2 and in the absence of NO . For this we calculate the reaction time for each of the three injector
 288 positions from pulsed addition of NO as described above, but normalized to the reaction time derived from addition of NO
 289 with numerical simulation. The results of such an experiment are displayed in Fig. 6 and we draw attention to the fact that,
 290 even at maximum reaction time (10.5 s), the change in the NO_3 concentration is only about 10 %. This reflects the low
 291 efficiency of reaction of NO_3 with the FEP coated glass walls. To put this result in context, performing the same experiment
 292 in a non-coated glass tube results in the almost complete loss of NO_3 . The numerical simulation was initialised with the same
 293 set of rate parameters described above, a fixed NO_2 concentration and only k_w and the initial NO_3 concentration were varied.
 294 The best fit was obtained when k_w was $4 \times 10^{-3} \text{ s}^{-1}$, in agreement with the simulations at fixed time and variable NO and NO_2 .
 295 Using expression (7), this value of k_w can be converted to an approximate uptake coefficient for NO_3 to the FEP-coated tube
 296 of $\approx 5 \times 10^{-7}$.

$$297 \quad \gamma = \frac{2 r k_w}{c} \quad (7)$$

298 3 Data analysis and derivation of NO_3 reactivity

299 We first consider the passage of NO_3 through the flow-tube in a flow of zero-air. If NO_3 is lost in one or more pseudo-first-
 300 order processes, its decay should be exponential and its concentration, $[\text{NO}_3]_t^{\text{ZA}}$ after a reaction time t , is given by expression
 301 (8).

$$302 \quad [\text{NO}_3]_t^{\text{ZA}} = [\text{NO}_3]_0^{\text{ZA}} \exp(-k_{\text{ZA}} t) \quad (8)$$



303 Where the superscript “ZA” refers to use of zero-air. As NO₃ is lost only via reaction with NO₂ and to the wall, $k_{ZA} =$
 304 $k_{\text{wall}} + k_{\text{NO}_2}$ where k_w is the first-order loss rate constant for wall-loss and k_{NO_2} is the first-order loss rate constant for
 305 reaction with NO₂ and is equal to $k_3[\text{NO}_2]$. When zero-air is switched for ambient air containing reactive trace gases (RTG),
 306 we have:

$$307 \quad [\text{NO}_3]_t^{\text{Amb}} = [\text{NO}_3]_0^{\text{Amb}} \exp(-k_{\text{Amb}}t) \quad (9)$$

308 where $k_{\text{Amb}} = k_w + k_{\text{NO}_2} + k_{\text{RTG}}$ and k_{RTG} is the first-order loss rate constant for reaction of NO₃ with trace gases present
 309 in ambient air other than NO₂.

310 If $[\text{NO}_3]_0^{\text{ZA}}$ and $[\text{NO}_3]_0^{\text{Amb}}$ are equivalent, expression 10 is obtained.

$$311 \quad \frac{[\text{NO}_3]_t^{\text{ZA}}}{\exp(-k_{\text{ZA}}t)} = \frac{[\text{NO}_3]_t^{\text{Amb}}}{\exp(-k_{\text{Amb}}t)} \quad (10)$$

312 Rearranging and substituting for k_{ZA} and k_{Amb} leads to

$$313 \quad k_{\text{RTG}} = \frac{\ln\left(\frac{[\text{NO}_3]_t^{\text{ZA}}}{[\text{NO}_3]_t^{\text{Amb}}}\right)}{t} = 1/\tau \quad (11)$$

314 Where τ is the NO₃ lifetime. In principal, it should thus be possible to calculate the reactivity of NO₃ in ambient air by
 315 measuring $[\text{NO}_3]_t^{\text{ZA}}$, $[\text{NO}_3]_t^{\text{Amb}}$ and knowing the reaction time t . Later we discuss the applicability of this expression and
 316 show that corrections are necessary to take the re-formation of NO₃ into account, especially when dealing with air-masses
 317 with high NO₂ content. This is similar to the laboratory experiments described above and required numerical simulation,
 318 which we present below.

319 The concentration of NO₃ in zero-air measured when the injector is positioned for maximum reaction time, $[\text{NO}_3]_t^{\text{ZA}}$, was
 320 measured by flushing the inlet with 3000 sccm zero-air creating an overflow of ≈ 100 sccm. When switching to ambient
 321 measurements, the zero-air overflow was redirected via a flow controller, F₃, that connected the zero-air overflow line to the
 322 exhaust and which was set to 3500 sccm. This setup has the advantage of enabling dynamic dilution of ambient air. If the
 323 reactivity is so high that the NO₃ levels approached the detection limit, F₃ does not withdraw the entire 3500 sccm overflow
 324 but allows e.g. 2000 sccm to be added to the inlet, resulting in sampling 900 sccm of ambient air plus 2000 sccm of zero-air,
 325 a dilution factor of 2900/900 which is slightly increased by the 400 sccm flow from the darkened reactor. A five point
 326 dynamic dilution with zero-air is implemented in the software, which changes the set point for F₃ and dilutes the ambient air
 327 with zero-air if $[\text{NO}_3]_t^{\text{Amb}}$ decreases below 10 pptv for an average time period of 30 s. Conversely, the dilution can be
 328 decreased again if $[\text{NO}_3]_t^{\text{Amb}}$ becomes $\geq [\text{NO}_3]_t^{\text{ZA}} - 10$ ppt. Dilution factors (D_i) were determined using a Gilibrator flow
 329 meter (Gilian Gilibrator-2) and were: D₁=1.14 for the measurement of pure ambient air (here the small dilution effect is
 330 caused by the 400 sccm zero-air used in the production of NO₃), D₂=1.74, D₃=3.71, D₄=8.98, D₅=14.07 when diluting
 331 ambient air. With increasing dilution, errors in the measurement will increase as well (see later).

332 The analytical expression given above to derive the NO₃ reactivity is an ideal case in which NO₃ is lost by a number of first-
 333 order processes and is not formed in the flow-tube to a significant extent. However, as we already demonstrated in the
 334 laboratory experiments to examine the effects of varying NO, NO₂ and NO₃ concentrations, the formation of N₂O₅ in the



335 reaction of NO_3 with NO_2 (R3) and its thermal decomposition back to NO_3 can impact on the NO_3 concentration as NO_2 is
336 present both in the mixture used to generate N_2O_5 and NO_3 and also in ambient air. While the formation of N_2O_5 from NO_2
337 and NO_3 (R2) is, to a good approximation, independent of temperature between about 280 and 305 K, the rate constant for
338 thermal decomposition of N_2O_5 (R3) varies by a factor of 26 over the same temperature range. The simple, analytical
339 approach outlined above thus fails at temperatures where the decomposition of N_2O_5 is important and when sufficient NO_2 is
340 present to account for a significant fraction of the loss of NO_3 . This is illustrated in Fig. 7a, in which simulations of the NO_3
341 concentration at a reaction time of 10.5 s and at different temperatures and amounts of NO_2 (as reactant) are displayed and
342 compared with the simple exponential behaviour (black data points) calculated from expression (11). The simulations show
343 that the dependence of the NO_3 concentration on NO_2 is non-exponential, indicating that re-generation of NO_3 from the N_2O_5
344 formed is significant, especially at higher temperatures. Figure 7b plots the ratio of the true reactivity (i.e. that used as input
345 into the numerical simulation) versus that obtained by analyzing the simultaneous change in NO_3 concentration using
346 expression (11). It is evident that the use of this expression generally results in underestimation of the true reactivity due to
347 the formation and decomposition of N_2O_5 . The bias will be largest when sampling polluted air where the reactivity has a
348 large component due to NO_2 and small under conditions of low NO_2 and high k_{RTG} typical for remote, forested areas.
349 However as previously mentioned the decomposition of N_2O_5 is strongly temperature dependent so that the bias will increase
350 with rising temperature and decrease with sinking flow-tube temperature.

351 Apart from the formation and thermal dissociation of N_2O_5 , the reaction of NO_2 with O_3 may, under some conditions,
352 represent a further potential source of NO_3 in the flow-tube despite the low rate constant for (R1). Due to the in-situ method
353 of production of N_2O_5 and NO_3 in the dark reactor, NO_2 (0.6-3 ppbv) and O_3 (40-50 ppbv) are always present in the flow-
354 tube. NO_3 generated in the flow-tube was therefore simulated for different amounts of O_3 and NO_2 corresponding to the
355 minimum and maximum mixing ratios used in our experiments. Figure 8 indicates that with 50 ppbv of O_3 and 2 ppbv NO_2 ,
356 < 0.5 pptv of NO_3 is formed in the 10.5 s available for reaction in the flow-tube, which would not strongly impact on the
357 results if the analytical expressions above were used to derive the NO_3 reactivity. Under highly polluted conditions (e.g. 100
358 ppbv O_3 and 20 ppbv NO_2) the effect is however measurable (> 2 pptv).

359 The discussion above indicates that the use of expression (11) can, under certain circumstances (e.g. low NO_x , high NO_3
360 reactivity to VOCs) give a reasonable representation of the NO_3 reactivity. However, in order to be able to derive NO_3
361 reactivities from any air mass we prefer to use numerical simulation take NO_3 reformation into account and enable extraction
362 of accurate values in any conditions.

363 3.1 Numerical simulations for extraction of ambient reactivity

364 In this section we outline the experimental procedure and the associated data analysis for extracting the NO_3 reactivity from
365 an ambient dataset as exemplified by the data shown in Fig. 9. This data covers a 1 hour period in which several phases of
366 inlet-overfilling with humidified zero-air and titration with NO are apparent as are periods of mixing NO_3 with ambient air.



367 The dataset has already been corrected for baseline drift in the NO₃ zero during titration, hence each titration-zero is
368 scattered around 0 pptv NO₃.

369 The periods marked “ZA” (zero-air) were used to extract the NO₃ concentration after a residence time of 10.5 s in flow-tube
370 in the absence of ambient reactive trace gases. The data show that a plateau in the NO₃ signal with zero-air is observed after
371 about 2-3 titration cycles are complete, which is the result of slow flushing through the inlet of reactive gases. Once a stable
372 signal is acquired, [NO₃]_{t=10.5}^{ZA} can be taken as an average value for each 300 s zero-air phase. These values are then used to
373 calculate the initial NO₃ concentration [NO₃]₀^{ZA}, i.e. before NO₃ enters the flow-tube. This was done in an interactive
374 procedure using numerical simulation with FACSIMILE embedded in a separate program. Input values are the O₃ and NO₂
375 concentration (from the darkened reactor), a first estimate for [NO₃]_{t=0}^{ZA} and the rate coefficients for the NO₃ reactions listed
376 in Table 1. At the end of the simulation (a few seconds of computing time) the simulated and measured values of [NO₃]_{t=10.5}^{ZA}
377 are compared and the ratio used to adjust the next input value for [NO₃]_{t=0}^{ZA}. The iteration continued until convergence was
378 reached. Convergence was considered satisfactory when the deviation between measured and simulated values of
379 [NO₃]_{t=10.5}^{ZA} was less ≤ 1 %. This usually took only 5 simulations per data point as the initial value for each new time point
380 was chosen to be the final value for the preceding time point. Ideally, [NO₃]_{t=0}^{ZA} should be constant over long periods of time.
381 In fact, deviations of several pptv, especially during field measurements, were observed over periods of hours and so values
382 of [NO₃]_{t=0}^{ZA} were linearly interpolated to each time point in which ambient reactivity was recorded.

383 Once initial NO₃ concentrations had thus been obtained a new set of simulations was started to simulate the measured values
384 of [NO₃]_{t=10.5}^{Amb}. In this case, the simulation was initialized with the values of [NO₃]_{t=0}^{ZA} obtained as described above and the
385 total NO₂ concentration and O₃ concentrations, which contained a constant contribution from the dark-reactor and a variable
386 concentration from ambient NO₂ and O₃ once corrected by the dilution factor (see above). An initial estimate of the total
387 NO₃ reactivity, *k*_{RTG}, was made and the simulated value of [NO₃]_{t=10.5}^{Amb} compared to that measured. The simulation was
388 iterated, with incremental adjustment of *k*_{RTG} until agreement between simulation was ≤ 1 %. For ambient datasets, in which
389 the reactivity can be highly variable this sometimes took several iterations, though as each simulation took less than a second
390 this is not a particularly time consuming procedure.

391 **4 Reactivity of an isoprene standard.**

392 To validate our experimental and analytical procedure, we performed reactivity measurements on a bottled isoprene standard
393 (0.933 ± 0.09 ppmv, Westfalen), diluted in zero-air. Isoprene was chosen as it is an important biogenic reactant for NO₃ in
394 the troposphere and also because the rate coefficient, *k*_{isoprene}, for its reaction with NO₃ has been studied on many occasions
395 (Atkinson et al., 2006; IUPAC, 2016) and therefore has a low associated uncertainty (*k*_{isoprene} = 6.5 ± 0.15 × 10⁻¹³ cm³
396 molecule⁻¹ s⁻¹ at 298 K).



397 Experiments were carried out at various isoprene and NO₂ mixing ratios and the results are summarized in Fig. 10, which
398 indicates excellent agreement between the measured reactivity and that calculated from the isoprene mixing ratio and rate
399 coefficient, the slope of an unweighted fit being 1.00 ± 0.03 . The error bars on the calculated reactivity represent total
400 uncertainty in the isoprene and NO₂ mixing ratio, the reaction time and the rate coefficient. These results confirm that the
401 instrument and data analysis procedure measure accurate values of NO₃ reactivity in the presence of NO₂ and organic
402 reactants.

403 **5 Detection Limit, dynamic range and overall uncertainty**

404 While the overall uncertainty associated with absolute NO₃ concentration measurement are influenced by factors such as
405 uncertainty in the cross-section as well as in the measurement of the laser emission spectrum the fractional change in
406 concentration used to derive the NO₃ reactivity is not impacted. The detection limit for measuring NO₃ reactivity is defined
407 by the minimal detectable change (MDC_{NO₃}) in the NO₃ mixing ratio. This depends on noise levels and drift in ring-down-
408 time, i.e. on the precision of the NO₃ signal and also on the stability of the synthetically generated NO₃. The instrumental
409 noise on the NO₃ signal was reduced by averaging over ≈ 3 s per data-point (≈ 1800 ring-down-events) to give a noise
410 limited detection limit of ≈ 0.2 pptv. Precision is limited by the stability of the CRDS setup where changes in the mirror
411 reflectivity induced by thermal or mechanical stress can lead to a drift in the ring-down time. The precision can be estimated
412 from the standard deviation of the signal from one zeroing period to the next over the measurement period. Under typical
413 laboratory conditions this was normally ≈ 0.7 pptv.

414 Since $[\text{NO}_3]_0^{\text{ZA}}$ is interpolated onto the measured $[\text{NO}_3]_t^{\text{Amb}}$ time series to calculate the reactivity, the stability of the NO₃
415 source is of great importance. Changes in the amount of synthetically generated NO₃ are caused by fluctuations in the
416 temperature or pressure of the dark-reactor, the flow of NO₂ and changes in the intensity of light from the O₃ generator. In
417 general, the poorer the stability of the NO₃ source chemistry, the more frequently the NO₃ mixing ratio in zero-air has to be
418 measured. In laboratory conditions, changes of ± 1 pptv within one hour were typical, making $[\text{NO}_3]_t^{\text{ZA}}$ measurements every
419 1200 s more than sufficient. In field conditions, where the instrument housing may be subject to larger temperature
420 fluctuations, more frequent determination of $[\text{NO}_3]_t^{\text{ZA}}$ may be necessary. The NO₃ source stability was obtained from the
421 standard deviation of the averaged $[\text{NO}_3]_t^{\text{ZA}}$ concentrations and propagating this with the standard deviation of two
422 consecutive $[\text{NO}_3]_t^{\text{ZA}}$ measurements, for which typical values in laboratory conditions were ≈ 1 ppt. To define an overall,
423 minimal detectable change in NO₃ (MDC_{NO₃}), the noise and drift limited precision was combined with the NO₃ source
424 stability to result in MDC_{NO₃} = 2.5 pptv.

425 An MDC_{NO₃} of 2.5 pptv results in a lower limit for the measurement of NO₃ reactivity of 0.005 s^{-1} (obtained from expression
426 (11) with $[\text{NO}_3]_t^{\text{ZA}} = 50$ pptv and $[\text{NO}_3]_t^{\text{Amb}} = [\text{NO}_3]_t^{\text{ZA}} - \text{MDC}_{\text{NO}_3} = 47.5$ pptv, at the lowest dilution factor of 1.14). An
427 upper limit for the measurable reactivity is 45 s^{-1} , largely defined by the uncertainty of the dilution factor. Dilution factors



428 were obtained by measurements of the actual flows going into the flow-tube using a Gilibrator flow meter (Gilian Gilibrator-
429 2, stated accuracy $\pm 1\%$). The total uncertainty in the dilution factor is defined by the accuracy of the measurement of the
430 dilution flows as well as by the accuracy of the flow controllers used for flow regulation ($\pm 2\%$) and was calculated to be
431 2.5 %. The error in the calculated reactivity is lowest for the lowest dilution but if the $[\text{NO}_3]_{\text{t}}^{\text{Amb}}$ gets close to the detection
432 limit this will also have a strong influence on the calculated reactivities making a higher dilution factor favourable. Dilution
433 factors were chosen to keep the instrument operating in a region ($10 \text{ pptv} < \text{NO}_3 < 40 \text{ pptv}$) where both effects are
434 minimized.

435 A minimum detectable change in NO_3 of 2.5 pptv leads to an uncertainty of $\approx 15\%$, when NO_3 varies between ≈ 10 und 30
436 pptv (starting from 50 pptv in zero-air). The uncertainty increases dramatically when NO_3 levels are close to 50 pptv (i.e.
437 very low reactivity) or less than 5 pptv (very high reactivity without dilution). This is illustrated in Figure S1 of the
438 supplementary information. As mentioned in section 2.3.1 the uncertainty in the reaction time (10 %) also contributes to the
439 overall uncertainty.

440 To assess the uncertainty associated with derivation of the NO_3 -reactivity from numerical simulation, uncertainties
441 associated with the input parameters have to be considered. As previously demonstrated (Groß et al., 2014) this is best
442 assessed in a Monte-Carlo approach in which the key parameters are varied within a range reflecting their uncertainty limits.
443 The parameters that most sensitively influence the derived value of NO_3 reactivity are the NO_2 mixing ratio and the rate
444 coefficients for N_2O_5 formation ($k_3 = 1.2 \pm 0.1 \times 10^{-12} \text{ cm}^3 \text{ molecule}^{-1} \text{ s}^{-1}$) and decomposition ($k_4 = 4.4 \pm 0.4 \times 10^{-2} \text{ cm}^3$
445 $\text{molecule}^{-1} \text{ s}^{-1}$). The rate coefficients listed are for 1 bar and room temperature as appropriate for the experimental conditions,
446 the uncertainties quoted ($\approx 10\%$) are based on assessment of kinetic data (Burkholder et al., 2016). The Monte Carlo
447 simulations were initiated with a NO_3 mixing ratio (in zero-air) of 50 pptv, decreasing to 20 pptv upon reaction with air. In
448 total, 6 sets of ≈ 1200 simulations were carried with variation of the initial NO_2 mixing ratio between 1 and 5 ppbv and the
449 associated error in NO_2 mixing ratio was taken as 8 %. For any given simulation, the output value of the NO_3 reactivity
450 (k_{RTG}) was stored. The 2σ uncertainty was derived from the Gaussian fits to histograms of k_{RTG} (insets at $\text{NO}_2 = 1.0, 3.0$ and
451 5.0 ppbv) and is plotted (as a percent of k_{RTG}) versus $k_{\text{RTG}} / \text{NO}_2$. The latter may be considered a measure of whether NO_3
452 reacts predominantly with NO_2 to form N_2O_5 (k_3) or with reactive trace gases. Fig. 11 shows that the uncertainty associated
453 with the simulations is very sensitive to ambient NO_2 levels, varying between $> 100\%$ (at 5 ppbv NO_2 and a reactivity of
454 0.017 s^{-1}) to 3.1 % (at 1 ppbv NO_2 and a reactivity of 0.092 s^{-1}) of the extracted k_{RTG} . Clearly, the extraction of k_{RTG} is most
455 accurate in conditions of low NO_x and when NO_3 lifetimes are short (e.g. forested regions far from anthropogenic activity).
456 Another potential bias in the measurement is the temperature dependence of the rate constant of the reactions of trace gases
457 with NO_3 . Measurements were normally conducted at 20°C in the flow-tube whilst outside temperature can differ from this.
458 However, (unlike OH) the NO_3 reactions which dominate its reactivity involve addition to double bonds (e.g. of terpenes)
459 and are only weakly temperature dependent. Therefore, to a good approximation, this error can be neglected. Under



460 circumstances where the reactivity is known to be driven by reaction with reactive trace gases for which NO_3 has large
461 temperature dependence this error has to be taken into consideration.

462 The overall uncertainty thus derives from a combination of measurement errors (cavity instability, drift in NO_3 source etc.)
463 and the need to correct for NO_3 reactions with NO_2 . Under ideal conditions (e.g. as described above for laboratory operation)
464 the former can be reduced to $\approx 16\%$. For a scenario in which biogenic VOCs dominate NO_3 reactivity in a low NO_x
465 (< 1 ppbv) environment an additional uncertainty of ≈ 6 -10 % from the numerical simulations results in a total uncertainty of
466 ≈ 17 -20 %. In a high NO_x environment, the total uncertainty will be dominated by that associated with the simulations. For
467 example, at 5 ppbv NO_2 and a reactivity of 0.03 s^{-1} the total error would be close to 45-50 %.

468 **6 Deployment in the NOTOMO campaign, 2015**

469 The NO_3 reactivity set-up described above was deployed for the first time in the field during the NOTOMO campaign
470 (NOcturnal chemistry at the Taunus Observatorium: insights into Mechanisms of Oxidation) in the Taunus mountains (S.W.
471 Germany) in 2016. The site, previously described in detail (Crowley et al., 2010; Sobanski et al., 2016b), is situated on top of
472 the “Kleiner Feldberg” mountain (850 m above sea level) in a forested area with urban influence. The site is impacted by
473 biogenic emissions from forested regions (mainly in the north/west) and by anthropogenic emissions from the local urban
474 centres of Frankfurt, Mainz and Wiesbaden in the south-east to south-west.

475 **6.1 Reactivity measurements during NOTOMO**

476 The NO_3 reactivity instrument was located in a research container and sampled from a common, high-flow inlet together
477 with other instruments. The high-flow inlet was driven by an industrial fan drawing $10 \text{ m}^3 \text{ min}^{-1}$ through a 15 cm diameter
478 stainless steel pipe with its opening about 8 m above the ground. This flow was sub-sampled with a 4 m length of ¼-inch
479 PFA tubing that extracted the required 3300 sccm air from the centre of the stainless steel pipe and directed it through a 1
480 μm PFA filter to the NO_3 -reactivity instrument. Due to thermostat break-down during NOTOMO, the NO_3 -reactivity
481 measurements were performed with the flow-tube at container temperature, which was variable (14 - 31 °C).

482 Previous campaigns at the Taunus Observatory have revealed occasionally high night-time mixing ratios of NO_3 and N_2O_5
483 (Sobanski et al., 2016b). As sampling NO_3 and N_2O_5 from ambient air would bias the NO_3 -reactivity measurements to low
484 values, a 2 l glass flask heated to ≈ 40 -50 °C was placed at night in the ambient air stream to decompose N_2O_5 to NO_3 and
485 NO_2 . Based on its thermal dissociation rate coefficient (0.75 s^{-1} at 50 °C), N_2O_5 completely decomposes within the ≈ 40 s
486 residence time in this glass vessel, and the NO_3 formed is expected to be lost on the uncoated glass walls, thus preventing
487 reformation of N_2O_5 . Measurements with ≈ 200 pptv of N_2O_5 added directly to the heated vessel and measured by the
488 ambient and heated channels of the two-cavity CRDS (see section 2.2) confirmed that neither NO_3 nor N_2O_5 survived. As the
489 N_2O_5 mixing ratio was measured during NOTOMO it is in principal possible to correct the data for the additional NO_2 thus
490 generated. However, on most nights N_2O_5 levels were too low for this to have a significant effect. Further experiments with



491 isoprene and α -pinene indicated that there was no significant change in NO_3 -reactivity when the glass vessel was used or not,
 492 indicating no significant losses of these VOCs in the glass flask. We cannot exclude that other, less volatile organic trace
 493 gases including e.g. acids or peroxides may be lost in the glass vessel, but these are not expected to contribute significantly
 494 to NO_3 losses as their rate coefficients for reaction with NO_3 are generally too low. A further potential bias related to the use
 495 of the glass trap is the thermal decomposition of PAN and related peroxy nitrates, which can acquire concentrations of up to
 496 a few ppb at this site (Thieser et al., 2016; Sobanski et al., 2016c). If PAN decomposes in the glass vessel NO_2 will form,
 497 thus contributing to the measured reactivity. Simulations indicate that during the 40 s residence time in the heated flask (at
 498 50 °C) only a small fraction ($\approx 2.6\%$) of the PAN decomposes to form NO_2 . For future experiments in environments of high
 499 NO_x with N_2O_5 and NO_3 present, the system will be operated at a lower temperature (e.g. 35 °C, $\tau_{\text{PAN}} = \sim 500$ s, $\tau_{\text{N}_2\text{O}_5} = \sim 6$ s)
 500 to make sure all of the $\text{N}_2\text{O}_5/\text{NO}_3$ is removed but PAN is preserved. We note that when measuring NO_3 -reactivity in regions
 501 with large biogenic emissions, the use of the glass vessel to remove NO_3 and N_2O_5 is generally not necessary as high levels
 502 of biogenic VOCs and the low levels of NO_x often found in forested / rural environments remote from anthropogenic
 503 influence will result in very low levels of NO_3 or N_2O_5 .

504 During NOTOMO, ambient levels of NO_2 , NO_3 , N_2O_5 and organic nitrates were measured with the CRDS instruments
 505 previously described by Sobanski et al. (Sobanski et al., 2016a; Thieser et al., 2016). The uncertainty in the measurements
 506 was 8 % for NO_2 , 20 % for NO_3 whereas the uncertainty for PAN was highly variable for each data point (Sobanski et al.,
 507 2016c). The O_3 mixing ratios were measured using a dual beam ozone monitor (2B-Technology Model 202) with an
 508 uncertainty of 2 %. $[\text{NO}]$ was not directly measured but its day-time concentration was calculated assuming photo-
 509 stationary-state via expression (12):

$$510 \quad [\text{NO}]_{\text{calc}} = J(\text{NO}_2) [\text{NO}_2] / k_{(\text{NO}+\text{O}_3)}[\text{O}_3] \quad (12)$$

511 where $J(\text{NO}_2)$ is the photolysis frequency of NO_2 and $k_{(\text{NO}+\text{O}_3)}$ is the rate constant for reaction of NO with O_3 . This expression
 512 ignores the oxidation of NO to NO_2 via e.g. reactions of peroxy radicals and thus overestimates NO . $J(\text{NO}_2)$ was measured
 513 using a spectral radiometer located close to the inlet (MetCon).

514 In this manuscript we focus on a three-day period, during which NO_3 -reactivity was measured (Fig. 12a). The NO_3
 515 reactivity, k_{RTG} , varied from 0.005 to 0.1 s^{-1} during night-time but reached values as high as 1.4 s^{-1} during day-time. The total
 516 uncertainty of the measurement is depicted by the green, shaded area. The red line indicates that, as expected, day-time
 517 losses are dominated by reaction with NO (up to 1.3 s^{-1}). Night-time values of k_{RTG} were between 0.005 and 0.1 s^{-1} .
 518 Assuming that NO levels are close to zero as measured previously at this site during night-time (Crowley et al., 2010), k_{RTG}
 519 is then expected to be dominated by VOCs.

520 In Fig. 12b, we compare values of k_{RTG} obtained by rigorous data correction (black curve), to those calculated directly from
 521 expression (11) (blue curve). The simple analytical expression (blue line) results in an underestimation of the reactivity,
 522 especially during night, when the overall reactivity is low, and in periods of high $[\text{NO}_2]$. Owing to lack of temperature
 523 stabilization of the darkened reactor (at this time not yet incorporated) and break-down of the flow-tube thermostat during
 524 the campaign, temperature fluctuations in the container resulted in $\text{MDC}_{\text{NO}_3} = 5.6$ pptv and hence an average, measureable



525 reactivity of $\approx 0.01 \text{ s}^{-1}$ during the campaign. As described in section 5 the minimum detectable change in NO_3 was combined
526 with the uncertainty associated with the dilution factor, reaction time, $[\text{NO}_2]$, $[\text{PAN}]$ and rate constants used to calculate the
527 overall uncertainty for the reactivity at every data point. The overall uncertainty for the measurement period illustrated in
528 Fig. 12 was $\approx 25 \%$.

529 In Fig. 13a/b we compare the measured night-time NO_3 -reactivity with that obtained from the stationary-state analysis using
530 expression (1). For the two nights in the period analysed, NO_3 mixing ratios were between 5 and 37 pptv ($[\text{NO}_3] \gg 5 \text{ pptv}$)
531 and the calculated stationary-state loss rate coefficients varied between $0.03\text{-}0.003 \text{ s}^{-1}$ compared to the measured reactivity
532 which was between $0.05\text{-}0.006 \text{ s}^{-1}$ with a short time period in which k_{RTG} fell below the detection limit of the instrument.
533 Within the total uncertainty, the measured and stationary-state reactivities are in reasonable agreement for most of the night
534 from the 17th to the 18th. From the night 18th to the 19th the stationary-state reactivity is much lower (up to a factor of eight)
535 than that measured. This difference and also the higher variability can be attributed to rapid variations in concentrations of
536 VOCs at the inlet (due e.g. to emissions from nearby trees) that are not considered in the stationary-state approach; i.e. very
537 local emissions of reactive gases will result in breakdown of the stationary-state assumption leading to the underestimation
538 of the reactivity of the local mixture of VOCs and NO_x . As the direct measurement of the NO_3 reactivity with this device
539 sums over all VOCs present in the air mass sampled, it should give the same result as summing each VOC concentration
540 multiplied by the individual rate coefficients for reaction with NO_3 , i.e. NO_3 reactivity = $\sigma [\text{VOC}]_i k_i$. As demonstrated
541 previously for this mountain site (Sobanski et al., 2016b), summed losses based on measurement of VOCs can significantly
542 exceed the reactivity based on a stationary-state analysis especially under some meteorological situations in which a low-
543 lying residual layer (with high NO_3 concentrations) influences the measurement.

544 **7 Conclusion and outlook**

545 We present the first instrument for measurement of NO_3 reactivity in ambient air. The flow-tube based instrument, utilizes
546 the depletion of synthetically generated NO_3 when mixed with ambient air and has a dynamic range of 0.005 s^{-1} to 45 s^{-1} .
547 Following intensive laboratory characterization to determine the effective reaction time, the wall loss constant of NO_3 and
548 the effect of NO_3 formation and reformation in the flow-tube, it was successfully tested against an isoprene standard. The
549 overall uncertainty depends on the relative rate of reaction of NO_3 with NO_2 or with other traces gases (e.g. VOCs or NO)
550 that do not generate N_2O_5 and which, under ideal conditions, is close to 15 %. The instrument is thus best suited for
551 measurement of NO_3 reactivity in regions with high biogenic activity and relatively low direct anthropogenic emissions of
552 NO_x , i.e. regions where the measurement of NO_3 concentrations is difficult owing to low production rates and a high loss
553 term.

554 First deployment of the instrument was during the NOTOMO observational experiment in summer 2015 at a forested,
555 mountain site with urban influence. The measured NO_3 reactivity ranged from 0.006 to 0.1 s^{-1} at night-time and reached
556 values as high as 1.4 s^{-1} during day-time. As expected, day-time reactivity was dominated by reaction with NO while night-



557 time reactivity involved other (presumably organic) trace gases. A comparison with stationary-state calculations of the NO_3
558 reactivity revealed poor agreement on occasions, presumably related to very local emissions causing a breakdown of the
559 stationary-state assumption.

560 Improvements to the dynamic range of the instrument require further stabilization of the NO_3 source and cavity-optics to
561 reduce the minimal detectable change in NO_3 (presently $\text{MDC}_{\text{NO}_3} = 2.5$ pptv). This could also be achieved by the use of
562 larger volume flow-tubes. Future deployment with simultaneous measurements of NO_3 , NO_2 , O_3 and VOCs will be
563 conducted to compare direct measurements of NO_3 reactivity with those obtained from the stationary-state approach and also
564 those calculated from summing losses to individual VOCs.

565 **Acknowledgements**

566 We would like to thank Heinz Bingemer and the staff and department of the Johann Wolfgang Goethe–University, Frankfurt
567 am Main for logistical support and access to the Taunus Observatory during NOTOMO. We also would like to thank Eva
568 Pfannerstil for providing the isoprene standard. We thank DuPont for the sample of FEP used to coat the walls of the flow
569 tube and darkened reactor. This work was carried out in partial fulfilment of the PhD (Johannes Gutenberg University,
570 Mainz, Germany) of Jonathan Liebmann.

571



572

573 **References**

- 574 Atkinson, R.: Atmospheric chemistry of VOCs and NO_x, *Atmos. Env.*, 34, 2063-2101, 2000.
- 575 Atkinson, R., and Arey, J.: Gas-phase tropospheric chemistry of biogenic volatile organic compounds: a review, *Atmos. Env.*, 37, S197-
576 S219, 2003a.
- 577 Atkinson, R., and Arey, J.: Atmospheric degradation of volatile organic compounds, *Chem. Rev.*, 103, 4605-4638, 10.1021/cr0206420,
578 2003b.
- 579 Atkinson, R., Baulch, D. L., Cox, R. A., Crowley, J. N., Hampson, R. F., Hynes, R. G., Jenkin, M. E., Rossi, M. J., and Troe, J.: Evaluated
580 kinetic and photochemical data for atmospheric chemistry: Volume I - gas phase reactions of Ox, HOx, NO_x and SO_x species, *Atmos.*
581 *Chem. Phys.*, 4, 1461-1738, 2004.
- 582 Atkinson, R., Baulch, D. L., Cox, R. A., Crowley, J. N., Hampson, R. F., Hynes, R. G., Jenkin, M. E., Rossi, M. J., and Troe, J.: Evaluated
583 kinetic and photochemical data for atmospheric chemistry: Volume II - reactions of organic species, *Atmos. Chem. Phys.*, 3625-4055,
584 2006.
- 585 Berden, G., Peeters, R., and Meijer, G.: Cavity ring-down spectroscopy: Experimental schemes and applications, *International Reviews in*
586 *Physical Chemistry*, 19, 565-607, 2000.
- 587 Brown, S. S., Stark, H., and Ravishankara, A. R.: Cavity ring-down spectroscopy for atmospheric trace gas detection: application to the
588 nitrate radical (NO₃), *Applied Physics B-Lasers and Optics*, 75, 173-182, 2002.
- 589 Brown, S. S., Stark, H., and Ravishankara, A. R.: Applicability of the steady state approximation to the interpretation of atmospheric
590 observations of NO₃ and N₂O₅, *J. Geophys. Res. -Atmos.*, 108, Art. 4539, 10.1029/2003JD003407, 2003.
- 591 Brown, S. S., Dube, W. P., Osthoff, H. D., Stutz, J., Ryerson, T. B., Wollny, A. G., Brock, C. A., Warneke, C., De Gouw, J. A., Atlas, E.,
592 Neuman, J. A., Holloway, J. S., Lerner, B. M., Williams, E. J., Kuster, W. C., Goldan, P. D., Angevine, W. M., Trainer, M., Fehsenfeld, F.
593 C., and Ravishankara, A. R.: Vertical profiles in NO₃ and N₂O₅ measured from an aircraft: Results from the NOAA P-3 and surface
594 platforms during the New England Air Quality Study 2004, *J. Geophys. Res. -Atmos.*, 112, D22304, doi: 10.1029/2007jd008893, 2007a.
- 595 Brown, S. S., Dube, W. P., Osthoff, H. D., Wolfe, D. E., Angevine, W. M., and Ravishankara, A. R.: High resolution vertical distributions
596 of NO₃ and N₂O₅ through the nocturnal boundary layer, *Atmos. Chem. Phys.*, 7, 139-149, 2007b.
- 597 Brown, S. S., Dube, W. P., Fuchs, H., Ryerson, T. B., Wollny, A. G., Brock, C. A., Bahreini, R., Middlebrook, A. M., Neuman, J. A.,
598 Atlas, E., Roberts, J. M., Osthoff, H. D., Trainer, M., Fehsenfeld, F. C., and Ravishankara, A. R.: Reactive uptake coefficients for N₂O₅
599 determined from aircraft measurements during the Second Texas Air Quality Study: Comparison to current model parameterizations, *J.*
600 *Geophys. Res. -Atmos.*, 114, art. D00F10, 10.1029/2008JD011679, 2009.
- 601 Brown, S. S., and Stutz, J.: Nighttime radical observations and chemistry, *Chem. Soc. Rev.*, 41, 6405-6447, 2012.
- 602 Burkholder, J. B., Sander, S. P., Abbatt, J., Barker, J. R., Huie, R. E., Kolb, C. E., Kurylo, M. J., Orkin, V. L., Wilmouth, D. M., and Wine,
603 P. H.: Chemical Kinetics and Photochemical Data for Use in Atmospheric Studies, Evaluation No. 18," JPL Publication 15-10, Jet
604 Propulsion Laboratory, Pasadena, <http://jpldataeval.jpl.nasa.gov>, 2016.
- 605 Crowley, J. N., Schuster, G., Pouvesle, N., Parchatka, U., Fischer, H., Bonn, B., Bingemer, H., and Lelieveld, J.: Nocturnal nitrogen oxides
606 at a rural mountain site in south-western Germany, *Atmos. Chem. Phys.*, 10, 2795-2812, 2010.
- 607 Crowley, J. N., Thieser, J., Tang, M. J., Schuster, G., Bozem, H., Hasaynali Beygi, Z., Fischer, H., Diesch, J.-M., Drewnick, F., Borrmann,
608 S., Song, W., Yassaa, N., Williams, J., Pöhler, D., Platt, U., and Lelieveld, J.: Variable lifetimes and loss mechanisms for NO₃ and N₂O₅
609 during the DOMINO campaign: Contrast between marine, urban and continental air, *Atmos. Chem. Phys.*, 11, 10863-10870, 2011.
- 610 Crutzen, P.: A discussion of the chemistry of some minor constituents in the stratosphere and troposphere, *Pure and Applied Geophysics*,
611 106-108, 1385-1399, 1973.
- 612 Curtis, A. R., and Sweetenham, W. P.: Facsimile, AERE, Report R-12805, in, 1987.
- 613 Dentener, F. J., and Crutzen, P. J.: Reaction of N₂O₅ on tropospheric aerosols - Impact on the global distributions of NO_x, O₃, and OH, *J.*
614 *Geophys. Res. -Atmos.*, 98, 7149-7163, 1993.



- 615 Donahue, N. M., Clarke, J. S., Demerjian, K. L., and Anderson, J. G.: Free-radical kinetics at high pressure: A mathematical analysis of
 616 the flow reactor, *J. Phys. Chem.*, 100, 5821-5838, 1996.
- 617 Fry, J. L., Draper, D. C., Barsanti, K. C., Smith, J. N., Ortega, J., Winkle, P. M., Lawler, M. J., Brown, S. S., Edwards, P. M., Cohen, R.
 618 C., and Lee, L.: Secondary Organic Aerosol Formation and Organic Nitrate Yield from NO₃ Oxidation of Biogenic Hydrocarbons, *Env.*
 619 *Sci. Tech.*, 48, 11944-11953, 10.1021/es502204x, 2014.
- 620 Geyer, A., and Platt, U.: Temperature dependence of the NO₃ loss frequency: A new indicator for the contribution of NO₃ to the oxidation
 621 of monoterpenes and NO_x removal in the atmosphere, *J. Geophys. Res. -Atmos.*, 107, 4431, doi:10.1029/2001JD001215,
 622 10.1029/2001JD001215, 2002.
- 623 Groß, C. B. M., Dillon, T. J., Schuster, G., Lelieveld, J., and Crowley, J. N.: Direct kinetic study of OH and O₃ formation in the reaction of
 624 CH₃C(O)O₂ with HO₂, *The Journal of Physical Chemistry A*, 118, 974-985, doi:10.1021/jp412380z, 2014.
- 625 Guenther, A. B., Jiang, X., Heald, C. L., Sakulyanontvittaya, T., Duhl, T., Emmons, L. K., and Wang, X.: The Model of Emissions of
 626 Gases and Aerosols from Nature version 2.1 (MEGAN2.1): an extended and updated framework for modeling biogenic emissions,
 627 *Geoscientific Model Development*, 5, 1471-1492, 10.5194/gmd-5-1471-2012, 2012.
- 628 Heintz, F., Platt, U., Flentje, H., and Dubois, R.: Long-term observation of nitrate radicals at the tor station, Kap Arkona (Rugen), *J.*
 629 *Geophys. Res. -Atmos.*, 101, 22891-22910, 1996.
- 630 Howard, C. J.: Kinetic measurements using flow tubes, *J. Phys. Chem.*, 83, 3-9, 1979.
- 631 Huang, Y., Shen, H. Z., Chen, Y. L., Zhong, Q. R., Chen, H., Wang, R., Shen, G. F., Liu, J. F., Li, B. G., and Tao, S.: Global organic
 632 carbon emissions from primary sources from 1960 to 2009, *Atmos. Env.*, 122, 505-512, 10.1016/j.atmosenv.2015.10.017, 2015.
- 633 Huang, Y., Coggon, M. M., Zhao, R., Lignell, H., Bauer, M. U., Flagan, R. C., and Seinfeld, J. H.: The Caltech Photooxidation Flow Tube
 634 Reactor - I: Design and Fluid Dynamics, *Atmos. Meas. Tech. Discuss.*, 2016, 1-36, 10.5194/amt-2016-282, 2016.
- 635 IUPAC: Task Group on Atmospheric Chemical Kinetic Data Evaluation, (Ammann, M., Cox, R.A., Crowley, J.N., Jenkin, M.E.,
 636 Mellouki, A., Rossi, M. J., Troe, J. and Wallington, T. J.) <http://iupac.pole-ether.fr/index.html>, <http://iupac.pole-ether.fr/index.html>, 2016.
- 637 Kovacs, T. A., and Brune, W. H.: Total OH loss rate measurement, *J. Atmos. Chem.*, 39, 105-122, 10.1023/a:1010614113786, 2001.
- 638 Lelieveld, J., Butler, T. M., Crowley, J. N., Dillon, T. J., Fischer, H., Ganzeveld, L., Harder, H., Lawrence, M. G., Martinez, M.,
 639 Taraborrelli, D., and Williams, J.: Atmospheric oxidation capacity sustained by a tropical forest, *Nature*, 452, 737-740, 2008.
- 640 Lelieveld, J., Gromov, S., Pozzer, A., and Taraborrelli, D.: Global tropospheric hydroxyl distribution, budget and reactivity, *Atmos. Chem.*
 641 *Phys. Discuss.*, 2016, 1-25, 10.5194/acp-2016-160, 2016.
- 642 Mielke, L. H., Furgeson, A., and Osthoff, H. D.: Observation of ClNO₂ in a mid-continental urban environment, *Env. Sci. Tech.*, 45, 8889-
 643 8896, doi:10.1021/es201955u, 2011.
- 644 Mogensen, D., Gierens, R., Crowley, J. N., Keronen, P., Smolander, S., Sogachev, A., Nölscher, A. C., Zhou, L., Kulmala, M., Tang, M.
 645 J., Williams, J., and Boy, M.: Simulations of atmospheric OH, O₃ and NO₃ reactivities within and above the boreal forest, *Atmos. Chem.*
 646 *Phys.*, 15, 3909-3932, 10.5194/acp-15-3909-2015, 2015.
- 647 Ng, N. L., Brown, S. S., Archibald, A. T., Atlas, E., Cohen, R. C., Crowley, J. N., Day, D. A., Donahue, N. M., Fry, J. L., Fuchs, H.,
 648 Griffin, R. J., Guzman, M. I., Hermann, H., Hodzic, A., Iinuma, Y., Jimenez, J. L., Kiendler-Scharr, A., Lee, B. H., Luecken, D. J., Mao,
 649 J., McLaren, R., Mutzel, A., Osthoff, H. D., Ouyang, B., Picquet-Varrault, B., Platt, U., Pye, H. O. T., Rudich, Y., Schwantes, R. H.,
 650 Shiraiwa, M., Stutz, J., Thornton, J. A., Tilgner, A., Williams, B. J., and Zaveri, R. A.: Nitrate radicals and biogenic volatile organic
 651 compounds: oxidation, mechanisms and organic aerosol, *Atmos. Chem. Phys. Discuss.*, 2016, 1-111, 10.5194/acp-2016-734, 2016.
- 652 Orphal, J., Fellows, C. E., and Flaud, P. M.: The visible absorption spectrum of NO₃ measured by high-resolution Fourier transform
 653 spectroscopy, *J. Geophys. Res. -Atmos.*, 108, Art. Nr. 4077, doi:10.1029/2002JD002489, 2003.
- 654 Osthoff, H. D., Pilling, M. J., Ravishankara, A. R., and Brown, S. S.: Temperature dependence of the NO₃ absorption cross-section above
 655 298 K and determination of the equilibrium constant for NO₃ + NO₂ <-> N₂O₅ at atmospherically relevant conditions, *Phys. Chem. Chem.*
 656 *Phys.*, 9, 5785-5793, 2007.
- 657 Osthoff, H. D., Roberts, J. M., Ravishankara, A. R., Williams, E. J., Lerner, B. M., Sommariva, R., Bates, T. S., Coffman, D., Quinn, P.
 658 K., Dibb, J. E., Stark, H., Burkholder, J. B., Talukdar, R. K., Meagher, J., Fehsenfeld, F. C., and Brown, S. S.: High levels of nitryl
 659 chloride in the polluted subtropical marine boundary layer, *Nature Geoscience*, 1, 324-328, 2008.



- 660 Phillips, G. J., Tang, M. J., Thieser, J., Brickwedde, B., Schuster, G., Bohn, B., Lelieveld, J., and Crowley, J. N.: Significant
661 concentrations of nitryl chloride observed in rural continental Europe associated with the influence of sea salt chloride and anthropogenic
662 emissions, *Geophys. Res. Lett.*, 39, L10811, doi:10.1029/2012GL051912, 2012.
- 663 Riedel, T. P., Bertram, T. H., Crisp, T. A., Williams, E. J., Lerner, B. M., Vlasenko, A., Li, S. M., Gilman, J., de Gouw, J., Bon, D. M.,
664 Wagner, N. L., Brown, S. S., and Thornton, J. A.: Nitryl Chloride and Molecular Chlorine in the Coastal Marine Boundary Layer, *Env.*
665 *Sci. Tech.*, 46, 10463-10470, 10.1021/es204632r, 2012.
- 666 Rinne, J., Markkanen, T., Ruuskanen, T. M., Petaja, T., Keronen, P., Tang, M. J., Crowley, J. N., Rannik, U., and Vesala, T.: Effect of
667 chemical degradation on fluxes of reactive compounds – a study with a stochastic Lagrangian transport model, *Atmos. Chem. Phys.*, 12,
668 4843-4854, 2012.
- 669 Schuster, G., Labazan, I., and Crowley, J. N.: A cavity ring down / cavity enhanced absorption device for measurement of ambient NO₃
670 and N₂O₅, *Atmos. Meas. Tech.*, 2, 1-13, 2009.
- 671 Seeley, J. V., Jayne, J. T., and Molina, M. J.: High-Pressure Fast-Flow Technique for Gas-Phase Kinetics Studies, *Int. J. Chem. Kinet.*, 25,
672 571-594, 1993.
- 673 Sinha, V., Williams, J., Crowley, J. N., and Lelieveld, J.: The comparative reactivity method - a new tool to measure total OH reactivity in
674 ambient air, *Atmos. Chem. Phys.*, 8, 2213-2227, 2008.
- 675 Sobanski, N., Schuladen, J., Schuster, G., Lelieveld, J., and Crowley, J.: A 5-channel cavity ring-down spectrometer for the detection of
676 NO₂, NO₃, N₂O₅, total peroxy nitrates and total alkyl nitrates, *Atmos. Meas. Tech. Discuss.*, 2016, 1-32, 10.5194/amt-2016-191, 2016a.
- 677 Sobanski, N., Tang, M. J., Thieser, J., Schuster, G., Pöhler, D., Fischer, H., Song, W., Sauvage, C., Williams, J., Fachinger, J., Berkes, F.,
678 Hoor, P., Platt, U., Lelieveld, J., and Crowley, J. N.: Chemical and meteorological influences on the lifetime of NO₃ at a semi-rural
679 mountain site during PARADE, *Atmos. Chem. Phys.*, 16, 4867-4883, 10.5194/acp-16-4867-2016, 2016b.
- 680 Sobanski, N., Thieser, J., Schuladen, J., Sauvage, C., Song, W., Williams, J., Lelieveld, J., and Crowley, J. N.: Day- and Night-time
681 Formation of Organic Nitrates at a Forested Mountain-site in South West Germany, *Atmos. Chem. Phys. Discuss.*, submitted, 2016c.
- 682 Thieser, J., Schuster, G., Phillips, G. J., Reiffs, A., Parchatka, U., Pöhler, D., Lelieveld, J., and Crowley, J. N.: A two-channel, thermal
683 dissociation cavity-ringdown spectrometer for the detection of ambient NO₂, RO₂NO₂ and RONO₂, *Atmos. Meas. Tech.*, 9, 553-576, 2016.
- 684 Thornton, J. A., Kercher, J. P., Riedel, T. P., Wagner, N. L., Cozic, J., Holloway, J. S., Dube, W. P., Wolfe, G. M., Quinn, P. K.,
685 Middlebrook, A. M., Alexander, B., and Brown, S. S.: A large atomic chlorine source inferred from mid-continental reactive nitrogen
686 chemistry, *Nature*, 464, 271-274, 10.1038/nature08905, 2010.
- 687 Wayne, R. P., Barnes, I., Biggs, P., Burrows, J. P., Canosa-Mas, C. E., Hjorth, J., Le Bras, G., Moortgat, G. K., Perner, D., Poulet, G.,
688 Restelli, G., and Sidebottom, H.: The nitrate radical: Physics, chemistry, and the atmosphere, *Atmos. Env. A*, 25A, 1-206, 1991.
- 689
- 690
- 691

692 **Table 1:** Facsimile¹ Simulations

693

$\text{NO}_2 + \text{O}_3 \rightarrow \text{NO}_3 + \text{O}_2$	$k_1 = 3.52 \times 10^{-17} \text{ cm}^3 \text{ molecule}^{-1} \text{ s}^{-1}$	k_1
$\text{NO}_3 + \text{NO} \rightarrow 2 \text{NO}_2$	$k_2 = 2.60 \times 10^{-11} \text{ cm}^3 \text{ molecule}^{-1} \text{ s}^{-1}$	k_2
$\text{NO}_3 + \text{NO}_2 + \text{M} \rightarrow \text{N}_2\text{O}_5 + \text{M}$	$k_3 = 1.24 \times 10^{-12} \text{ cm}^3 \text{ molecule}^{-1} \text{ s}^{-1}$	k_3
$\text{N}_2\text{O}_5 + \text{M} \rightarrow \text{NO}_2 + \text{NO}_3 + \text{M}$	$k_4 = 4.44 \times 10^{-2} \text{ cm}^3 \text{ molecule}^{-1} \text{ s}^{-1}$	k_4
$\text{NO} + \text{O}_3 \rightarrow \text{NO}_2 + \text{O}_2$	$k_5 = 1.89 \times 10^{-14} \text{ cm}^3 \text{ molecule}^{-1} \text{ s}^{-1}$	k_5
$\text{NO}_3 + \text{wall} \rightarrow \text{NO}_2$	$k_w = 4 \times 10^{-3} \text{ s}^{-1}$	k_w
k_{RTG}	variable / fitted	k_{RTG}

694 ¹For all simulations FACSIMILE-CHEKMAT (Release H010 DATE 28.04.87 Version 1) was used. The rate constants (k_i) listed were
 695 taken from the IUPAC recommendations (Atkinson et al., 2004; IUPAC, 2016) at 298 K and 1 bar.

696



697
698
699
700
701

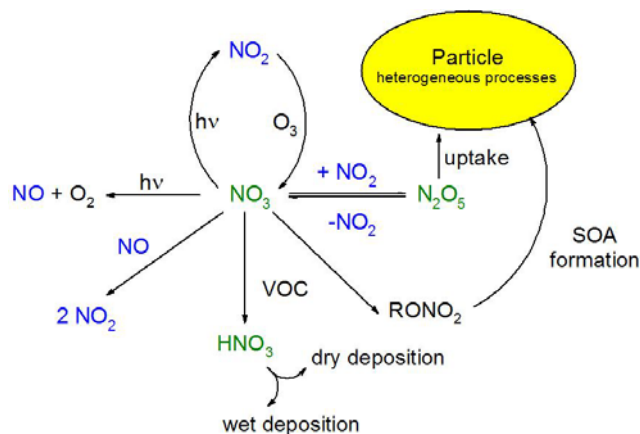


Figure 1: Gas-phase formation and loss of tropospheric NO_3 .
SOA = secondary organic aerosol, RONO_2 are alkyl-nitrates.

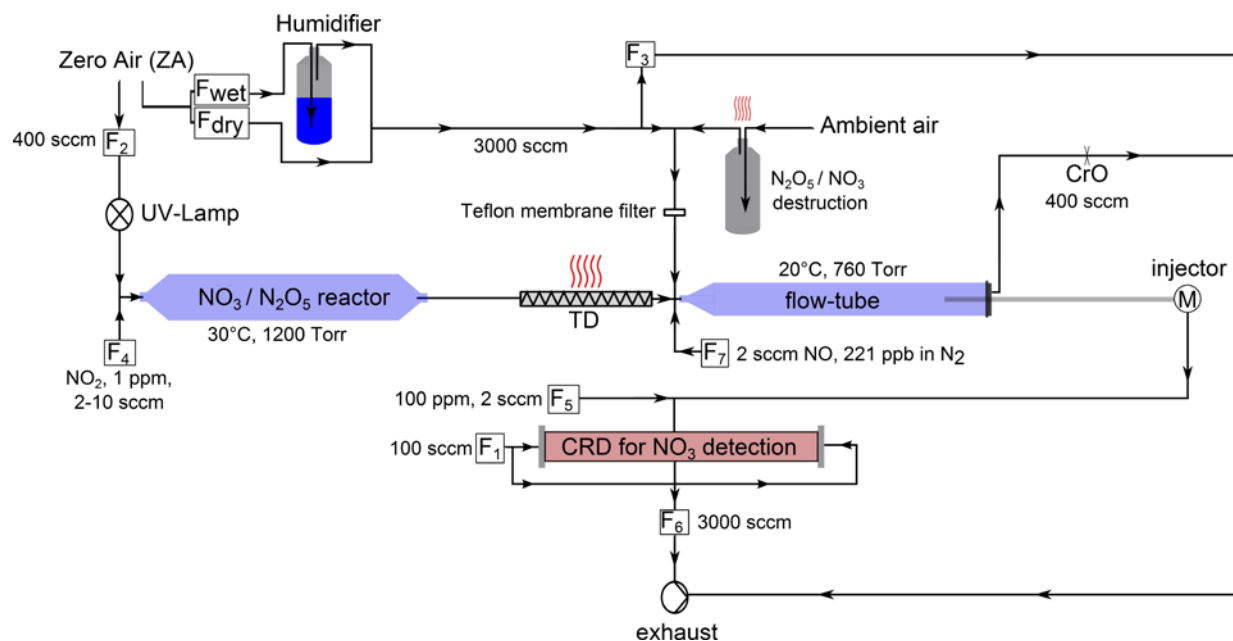


Figure 2: Schematic diagram of the NO_3 -reactivity measurement. F_1 - F_7 are mass flow-controllers: F_1 = mirror purge flow, F_2 = zero-air for O_3 generation, F_3 = dilution / inlet overflow (switching between zero-air and ambient), F_4 = NO_2 for NO_3 / N_2O_5 generation, F_5 = NO titration of NO_3 , F_6 = cavity flow to pump, F_7 = NO flow for online reactivity calibration. CrO = critical orifice. TD = heated tubing for thermal decomposition of N_2O_5 to NO_3 at 140 °C.



728
729
730
731
732
733
734
735
736
737
738
739
740
741
742
743
744
745
746
747
748
749
750
751
752
753
754
755

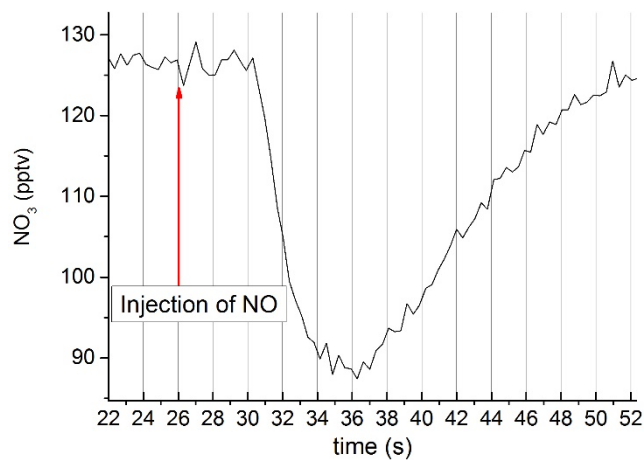


Figure 3: Derivation of effective reaction time by addition of a pulse (at $t = 26$ s) of NO using a syringe. The subsequent depletion in the NO₃ signal was analysed using expression 4.



756

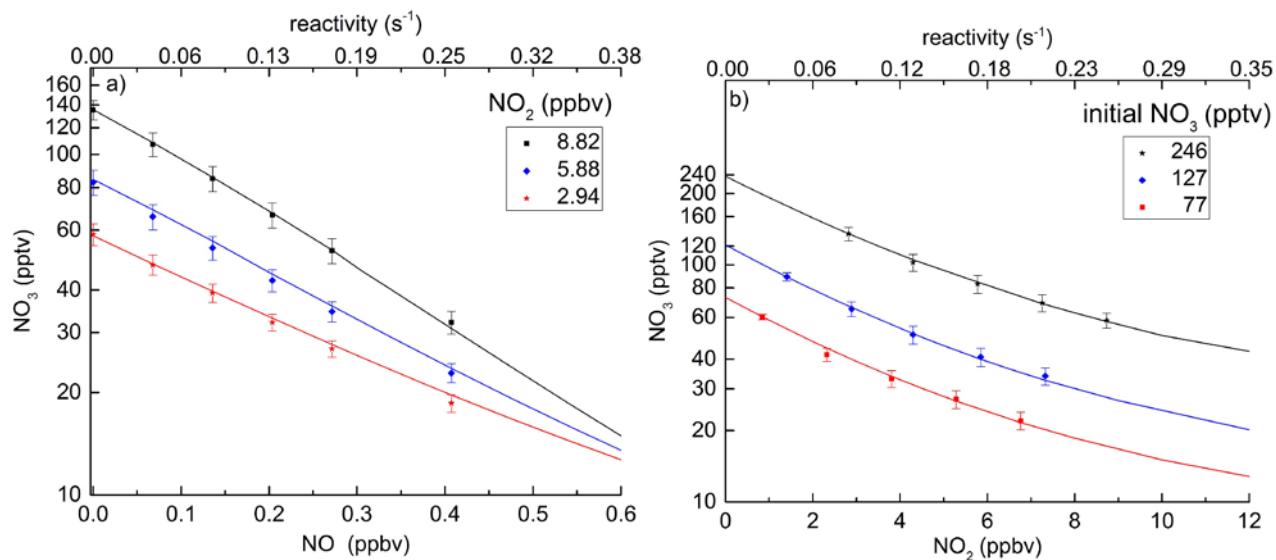


Figure 4: Characterisation of the flow-tube by numerical simulation of the NO_3 change following addition of NO and NO_2 at different mixing ratios. The symbols are measured NO_3 mixing ratios, the lines are the results of numerical simulations. The reactivity scales were calculated from $k_2[\text{NO}]$ and $k_3[\text{NO}_2]$ using the rate constants listed in Table 1.

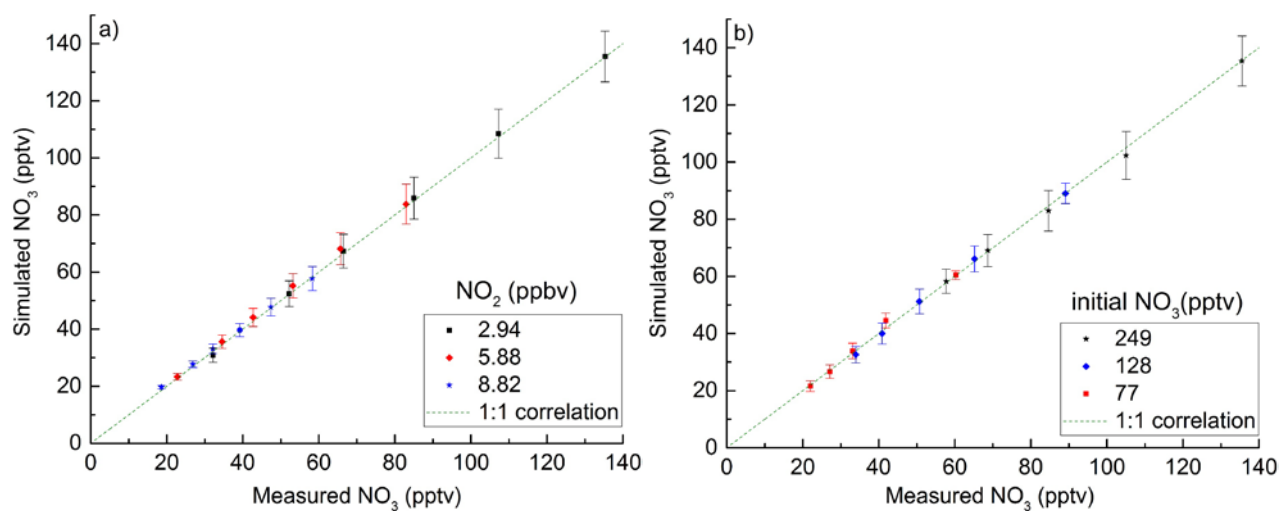


Figure 5: *Left:* Measured versus simulated $[\text{NO}_3]$ for different amounts of added NO (67, 134, 201, 268, 402 pptv) and at three different mixing ratios of NO_2 . *Right:* Measured versus simulated NO_3 (initially 77, 128 or 249 pptv) at different amounts (1.5, 3, 4.5, 6 ppbv) of added $[\text{NO}_2]$. The solid lines represent 1:1 agreement.



773
774
775
776
777
778
779
780
781
782
783
784
785
786
787
788
789
790

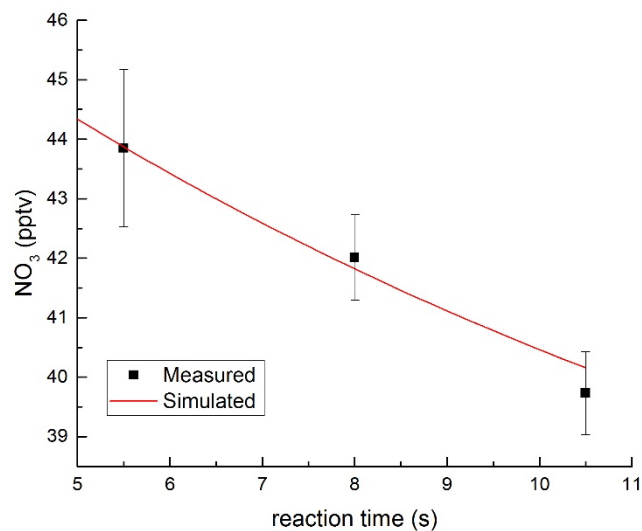


Figure 6: Determination of the wall loss constant of NO₃ by variation of the reaction time (injector position). The simulation indicates a wall loss constant of $k_w = 0.004 \text{ s}^{-1}$.

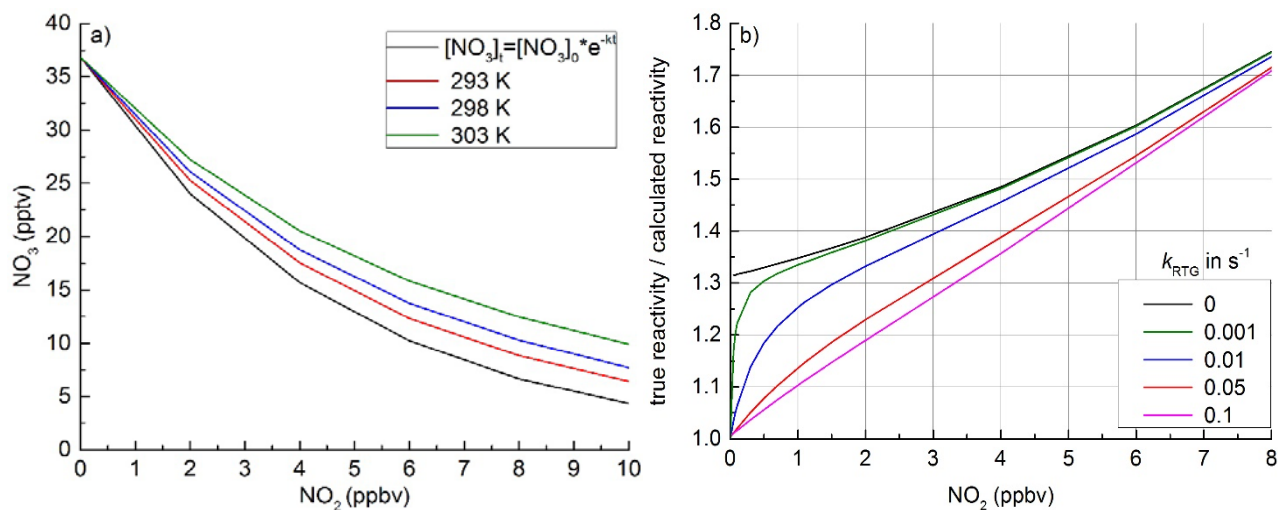


Figure 7: Influence of N_2O_5 formation and decomposition in the flow-tube. a) simulated (red, blue and green) mixing ratio of NO_3 versus added NO_2 at a reaction time of 10.5 s at various temperatures and thus thermal decomposition rates of N_2O_5 . The simple exponential decay of NO_3 (expression 9) is given by the black line. b) Effect of NO_2 level on the ratio of true reactivity / reactivity calculated from expression (8) for different loss rate constants for NO_3 reacting with reactive traces gases.



811
812
813
814
815
816
817
818
819
820
821
822
823
824
825
826
827
828

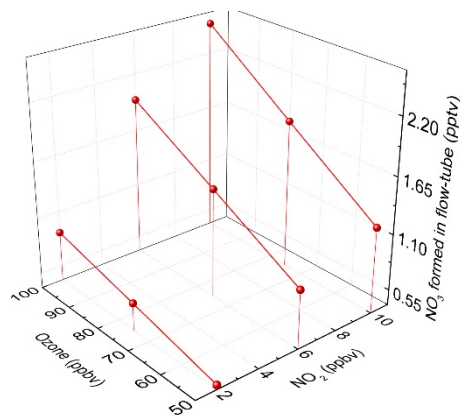


Figure 8: Simulated NO_3 production in the flow-tube at different O_3 and NO_2 mixing ratios at a fixed reaction time of 10.5 s.



829
830
831
832
833
834
835
836
837
838
839
840
841
842
843
844
845
846
847
848
849
850
851
852
853
854
855
856
857
858
859
860
861

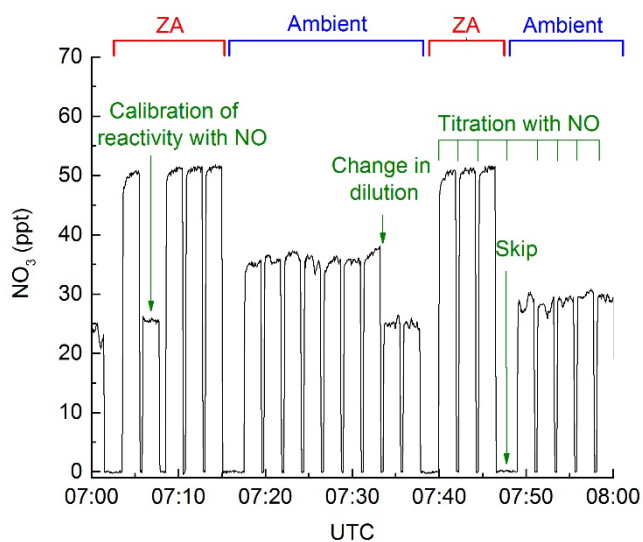


Figure 9: Raw data showing the change in NO₃ (10.5 s reaction time) between zero-air (ZA, periods marked with red brackets) and ambient air (Ambient, blue brackets). The Figure also shows periods of titration of NO₃ with NO (≈ 2 min intervals, green brackets), a change in the dilution factor from 4 to 3 (at ≈ 07:33) and an in-situ reactivity calibration (at ≈ 07:07). The “skip” periods are those in which data is not analysed due to switching from ambient air to zero-air and vice versa.



862

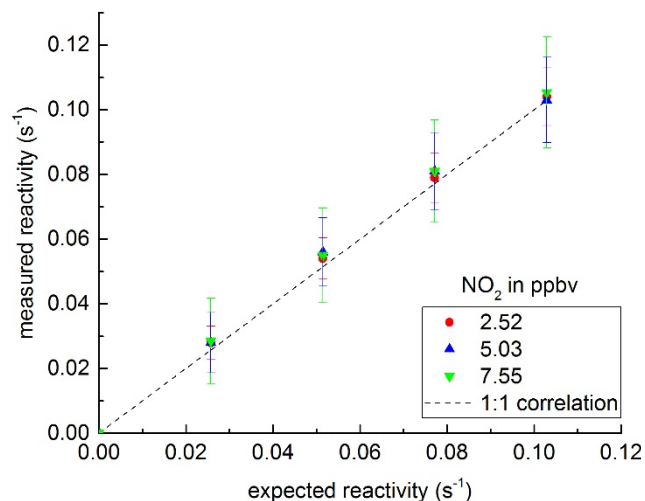


Figure 10: Verification of the experimental procedure by addition of isoprene at different NO₂ mixing ratios. The known reactivity was calculated from the isoprene mixing ratio (1.5 – 6 ppbv) and the rate coefficient for reaction of isoprene with NO₃. Experiments were performed in dry zero-air. The error bars in the simulation are due to uncertainties in [isoprene] and [NO₂] (both 5 %) and the reaction time (10 %).



863
864
865
866
867
868
869
870
871
872
873
874
875
876
877
878
879
880
881
882
883
884
885
886
887
888
889
890

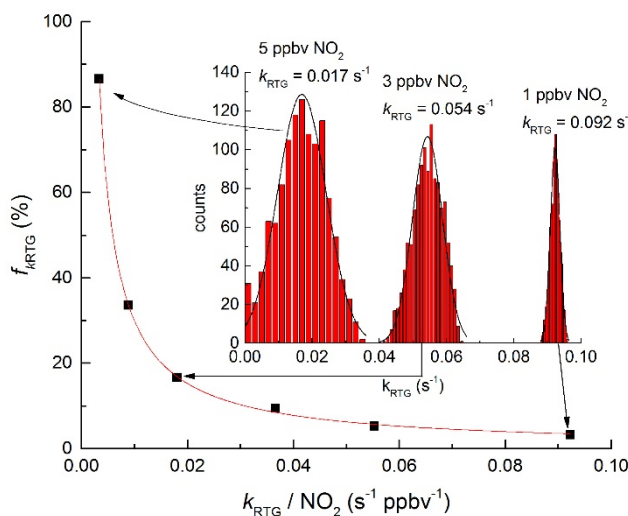


Figure 11: Uncertainty factor ($f_{k_{RTG}}$) as a function of the ratio $k_{RTG} / [NO_2]$ as derived from Monte-Carlo simulations. The relationship (red curve) is described by $f(k_{RTG}) = 0.33 \times (k_{RTG} / NO_2)^{-0.977}$. The results of three individual sets of 1200 simulations are shown as histograms.

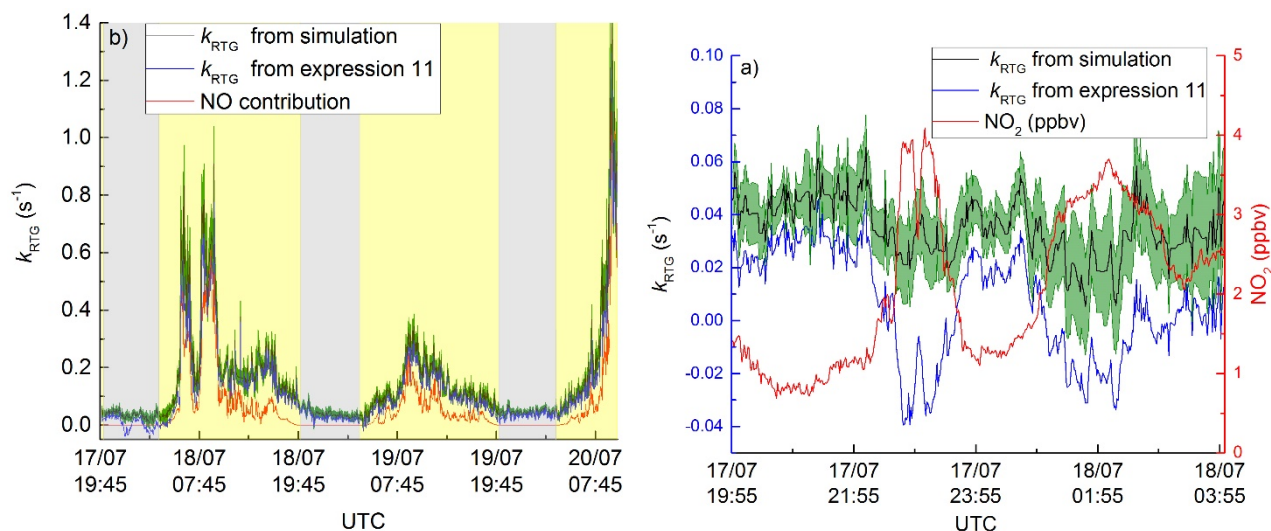


Figure 12: a) Measured values of k_{RTG} over a 3 day period. The overall uncertainty is represented by the green, shaded area. The black lines are k_{RTG} obtained by full simulations, the blue lines are calculated using expression (11) (without correction for N₂O₅ formation and decomposition). The contribution of NO to the NO₃ reactivity is displayed as the red line. Yellow regions correspond to day-time, grey regions correspond to night-time b) Zoom in on a night-time period with low reactivity emphasizing the effect of NO₂-induced formation and decomposition of N₂O₅.

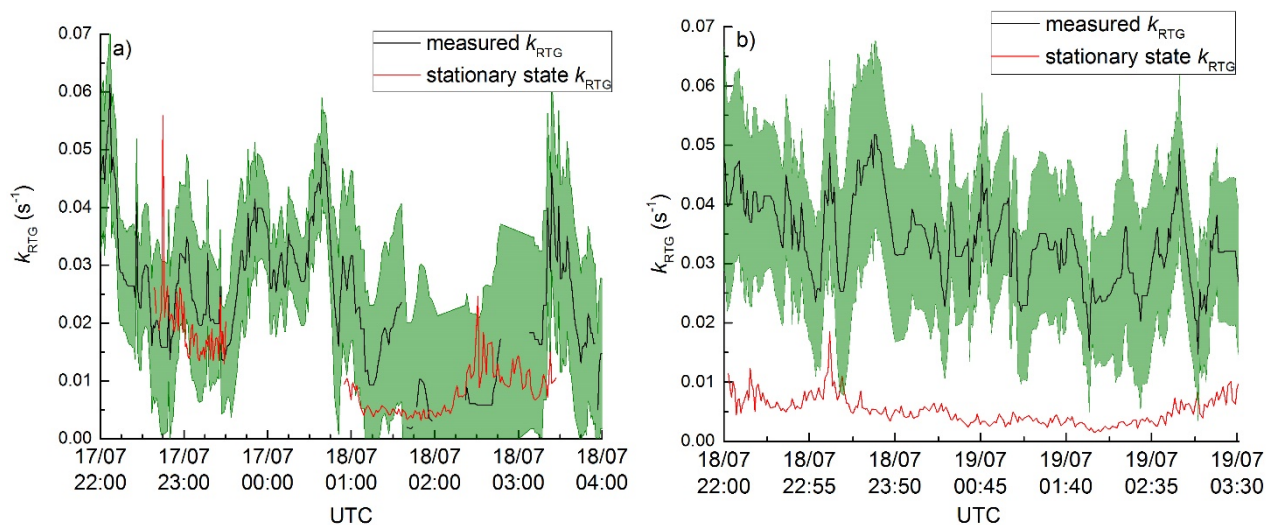


Figure 13: Comparison of stationary-state and measured NO_3 loss rates. Uncertainty in k_{RTG} (see text) are displayed as the green shaded areas.